NASA Contractor Report 4651

Euler Technology Assessment for Preliminary Aircraft Design Employing OVERFLOW Code With Multiblock Structured-Grid Method

David A. Treiber and Dennis A. Muilenburg
Boeing Defense & Space Group • Seattle, Washington

National Aeronautics and Space Administration
Langley Research Center • Hampton, Virginia 23681-0001

Prepared for Langley Research Center
under Contract NAS1-18762

March 1995

This publication is available from the following sources:

NASA Center for AeroSpace Information
800 Elkridge Landing Road
Linthicum Heights, MD 21090-2934
(301) 621-0390

National Technical Information Service (NTIS)
5285 Port Royal Road
Springfield, VA 22161-2171
(703) 487-4650

FOREWORD

This final report was prepared by the Boeing Defense & Space Group, Seattle, WA for the Langley Research Center, National Aeronautics and Space Administration, Hampton, VA. The work was performed under Contract No. NAS1- 18762, Task 26, "Euler Technology Assessment for Preliminary Design Applications to Sharp-Edged Configurations." Farhad Ghaffari was the Project Monitor on this contract.

Dr. J.A. Bossi of the Boeing Defense & Space Group was the Program Manager; D.A. Treiber and D.A. Muilenburg were the Principal Investigators.

The experimental data presented in this report are courtesy of Dr. Robert M. Hall of NASA Langley Research Center.

SUMMARY

The viability of applying a state-of-the-art Euler code to calculate aerodynamic forces and moments through maximum lift coefficient for a generic sharp-edge configuration is assessed. The OVERFLOW code, a method employing overset (Chimera) grids, was used to conduct mesh refinement studies, a wind tunnel wall sensitivity study, and a 22-run computational matrix of flow conditions, including sideslip runs and geometry variations. The subject configuration was a generic wing-body-tail geometry with a chined forebody, swept wing leading-edge, and deflected part-span leading-edge flap.

The analysis showed that the Euler method is adequate for capturing some of the non-linear aerodynamic effects resulting from leading-edge and forebody vortices produced at high angle-of-attack through $C_{L_{max}}$. Computed forces and moments, as well as surface pressures, match well enough for useful preliminary design information to be extracted. Vortex burst effects and vortex interactions with the configuration are also modeled.

CONTENTS

ILLUSTRATIONS

1.0 INTRODUCTION

Current high-performance fighter aircraft requirements of agility and supermaneuverability have led to the need to assess the characteristics of aircraft configurations at angles-of-attack beyond maximum lift coefficient early in the design process. Nonlinear aerodynamic effects are present in this regime however, where traditional preliminary design tools are of limited accuracy. Most configurations with swept, low-aspect ratio wings and oddly shaped forebodies depend on vortical effects which are not easily modeled by panel and full-potential methods commonly used in preliminary design. Advanced CFD tools capable of modeling detailed flow physics such as Navier-Stokes methods can be somewhat expensive and rather slow given the limited resources available to a typical preliminary design project.

Many configurations of interest, however, have special features resulting from high cruise speed and low-observable requirements such as sharp leading edges and chines. These features often control the position and strength of vortices present due to flow separation at high angle-of-attack. Since the Euler equations admit vorticity, and the truncation error and numerical properties present in most Euler methods lead to flow separation at sharp surface discontinuities, Euler methods offer a less expensive option for modeling high angle-of-attack flowfields.

This study examined the ability of an Euler method to model high angle-of-attack flows for a test configuration with the attributes described above in the context of obtaining information useful for preliminary design. The code used in the study was OVERFLOW, and the subject configuration was the Modular Transonic Vortex Interaction (MTVI) configuration, with geometry and wind tunnel test data supplied by NASA Langley Research Center.

The analysis techniques and approach are outlined, followed by the results of a mesh refinement and wind tunnel wall effects study. Then the effects of three different geometry variations (tail position, chine angle, and leading-edge flap angle) are examined, followed by conclusions.

2.0 ANALYSIS METHODOLOGY

2.1 Flow Solver

The analysis method used in this study utilizes one of a broad classification of Euler/Navier-Stokes codes known as overset mesh, or Chimera methods. This approach allows the flow domain to be decomposed into block structured grids that may overlap each other, as opposed to traditional block structured codes where the grid blocks abut on block faces in a more orderly fashion.

The Chimera approach offers several advantages. Complex configurations can be built up piecemeal, gridding each part independently and assembling the complete grid at the end. Configuration parts (wings, tails) can be added or removed without having to rework the remaining grid blocks. Since block boundaries and topologies can be specified arbitrarily, gridpoint distribution can be optimized and grid skewness minimized. The disadvantages are that since block boundary information must be obtained from the interior of adjacent blocks, adequate block overlap must be maintained, and this is not always straightforward. Adjacent blocks that contain abutting surfaces, such as a wing-body juncture, sometimes require special treatment because of difficulty in preserving proper overlap. Boundary information transfer is usually performed with a simple tri-linear interpolation scheme, so it is also important that the grid be smooth and that cells be of similar size at boundaries so that solution accuracy is not compromised.

The flow solver code used in the present analysis was OVERFLOW (1), a general purpose Euler/Navier-Stokes code provided by NASA Ames Research Center. The code is a Chimera version of ARC3D, and solves the steady-state Euler equations in a finite difference formulation. The inviscid flux terms are cast as second-order central differences, and the blended 2nd-4th order artificial dissipation scheme of Jameson is used for stability. The time advancement algorithm is the implicit diagonalized Beam-Warming approximate factorization method of Pulliam and Chaussee. The boundary conditions employed in the study were farfield conditions based on characteristic theory, and tangential flow with extrapolated static pressure was imposed at surface boundaries.

The code used for mesh generation was GRIDGEN2D/GRIDGEN3D (2), an interactive graphically driven gridding tool written at General Dynamics/Fort Worth. This code contains a host of methods for generating grids on prescribed surfaces and block boundary grids utilizing algebraic and elliptic solvers. GRIDGEN2D runs on an IRIS 4D graphics workstation, and GRIDGEN3D on an HP755 workstation.

Once the grids are generated, they must be pre-processed by another code, PEGSUS (3). This code, provided by AEDC, automatically identifies overset grid boundary points, creates user specified holes in the interior of grid blocks to accommodate configuration surfaces belonging to other blocks, and computes the interpolants and basis points for each overset boundary point.

2.2 Domain Decomposition and Mesh Generation

The MTVI configuration is a generic fighter-type geometry with a chined forebody and 60-deg cropped delta wing with a 2/3-span leading-edge flap deflected at 30-deg. Two different forebody sections were tested with included chine angles of 100-deg (MTVI1, MTVI2) and 30-deg (MTVI3). The model also has two different vertical tail arrangements. The twin tail case (MTVI1) has tails mounted on the wing at the 1/3-span location, and the single tail case (MTVI2) has the tail located on the afterbody centerline.

The geometry description as received from NASA Langley was modified slightly for convenience. The ends of the deflected leading-edge flap were extended or truncated to match the constant but-line wing break stations to eliminate the spanwise gap between the flap-outboard wing and flap-body junctures. Some surface network points were moved slightly to match points on adjacent surfaces to uniquely define geometry breaks common to adjacent gridblocks. None of these changes was expected to influence the calculations.

In developing the domain decomposition scheme, it was kept in mind that a grid refinement investigation was part of the study, that an extensive run matrix was called for in a limited amount of time, and that geometry changes would be required. This led to a conceptually simple scheme that would allow the geometry variations and grid coarsening and refinement without affecting the degree or quality of most of the block overlap boundaries. Quite often, the most severe stumbling block encountered in Chimera methods is obtaining a grid arrangement where all boundary points possess permissible overlap (no 'orphans'), and as adjacent grids become more coarse, the problem is magnified. It was thus decided to use h-topology grids extending away from configuration surfaces such that all boundary planes could be specified by a plane surface or configuration surface edge. In this way, as gridblocks are coarsened and refined in the normal direction, the grid boundaries do not move. Once valid block overlaps are established, they will still work for the coarse and fine grids.

Fig. 1 shows the configuration surface grid for the upper half of the geometry. 10 h-meshes surround the forebody, midbody, tail surfaces, and upper and lower wing surfaces and extend 15" away from the surface in the normal direction. Most of these blocks abut on planar surfaces. An o-mesh surrounds the sting and body aft of the wing trailing-edge and extends 15" away. Fig. 2 outlines some of the block boundaries on the upper half of the configuration. Blocks were extended algebraically as necessary, such as forward of the wing leading-edge and outboard of the side-of-body, to provide block boundary overlap.

Although at this point the entire domain is filled with points, there remain some areas which require special treatment. An example is the inboard boundary plane of the block residing over the wing upper surface and flap (Fig. 3). The points on this plane which lie below the side-of-body/body upper surface intersection, indicated by the arrows, should be surface boundary points instead of Chimera overlap points. It would be tedious to hunt down which of those points are below the line and difficult to supply proper boundary information input to OVERFLOW because gridlines in that plane cross the line arbitrarily. Also, the boundary points that lie both above the flap and below the lower side-of-body line must be specified such that flow can pass between the gap created by the deflected flap at the body and at the outboard flap tip. To treat these areas, small prism-shaped blocks were created whose faces match these base surfaces, lie on previously described surfaces, or lie entirely within the interior of another block (Fig. 4). While the fluid flow equations are solved within these blocks, their small size leads them to act mainly as interpolation stencil providers for the ambiguous boundary points of the larger blocks that they inhabit. Fig. 5 shows an example of the block wedged between the outboard wing/flap gap to allow flow through that region. To cover all these areas and the bases created by the wing and tail tips led to a total of 27 gridblocks covering the configuration surface, approximately 20,000 surface gridpoints, and took 8 hours to generate the complete surface mesh.

Extending the field mesh to the farfield was accomplished by adding a cartesian gridblock around the existing nearfield gridblocks. Fig. 6 shows the extent of all field grids on the centerline, and the hole in the outer block created by PEGSUS to accommodate the aircraft geometry. The complete extent of that hole is shown in Fig. 7. Since the most significant geometry change called for in this study was the repositioning of the vertical tail from the wing to the body centerline, it was convenient to create a hole in the block on the wing upper surface to accommodate the tail (Fig. 8) rather than dividing the inboard wing into 2 blocks.

The mesh resolution on the surface varied from a minimum of .1" (.5% of the root chord) near the wing leading-edge to .5" near the middle of the body. The minimum normal spacing at all surfaces for the medium resolution grid was .02" using 30 points in the normal direction per block. Coarse grid normal spacing at the surface was .05" using 15 points in the normal direction. Fine grid surface normal spacing was .01" using 60 points in the normal direction. For the medium resolution mesh, this gave a total of 668,000 points in the nearfield blocks. For the coarse mesh, the total was 485,000 points, and the fine mesh had 1,185,000 points. Including the outer cartesian block, the total numbers of points were 922,000, 739,000, and 1,439,000 respectively. The interior gridpoints were all generated algebraically with the 3-D transfinite interpolation option of GRIDGEN3D, and 40 hours were needed to complete the first mesh, including PEGSUS pre-processing.

The configuration geometry variations were quickly dispatched as follows. To move the tail from the wing to the body, the blocks surrounding the tail were moved to the body centerline, and a new Chimera hole was cut in the body upper surface and aftbody blocks. For the configuration with 30 degree forebody chine angle, the upper and lower forebody blocks were replaced. All blocks were algebraically reflected across the centerline to accomplish the runs in sideslip. The undeflected flap cases required the regeneration of the blocks above and below the inboard wing and removal of the blocks in the gaps at the flap tips.

3.0 RESULTS

3.1 Pathfinder Calculations

The pathfinder runs for this study consisted of two tests: an examination of the sensitivity of results due to grid refinement at low and high angles-of-attack, and the effect of including the wind tunnel walls in the calculation. For these runs and the runs that follow in this study, OVERFLOW was run at the recommended dissipation settings. Time was advanced a constant CFL number of 5., and all runs were at a freestream Mach number of .4. llMW of main memory were needed to accommodate the largest gridblock, and about 30MW of SSD were used to store block information during the runs. The code was compiled using the multi-tasking facility on the NAS C-90. Using 8 concurrent processors, a 1,500 iteration run took 2.4 CPU hours and about 1 hour wall clock time to complete. The low angle-of-attack runs converged 3 orders-of-magnitude in L2-Norm residual over this period. The high alpha runs converged 1 order-of-magnitude and were somewhat unsteady. The convergence histories shown in Figs. 9a,b are typical for runs performed below and above $C_{L_{max}}$ respectively. Each line is the L2-Norm of an individual gridblock. Fig. 9c shows the variation of lift coefficient over 1,000 iterations for the medium grid at 35 deg. angle-of-attack. One case was advanced past 4,000 iterations with no significant changes in flow properties or forces and moments, so it was concluded that 1,500-2,000 iterations was adequate for all proceeding cases.

The results of the grid sensitivity study are shown in Fig. 10. At both low and high alpha, all grids show reasonable agreement with test data in lift and drag. Pitching moment varies somewhat, and at the high angle-of-attack is significantly off. Since the 35-degree runs for all grids were unsteady, a conclusion about which grid adequately resolves the flow at this alpha is difficult to make. The lift varied enough in the steady-state limit cycle such that any one of the calculations could match test data depending on exactly where it was stopped. Since all grids modeled the principal flow features to some degree, and forces and surface pressures compared well with test data, it was concluded that the medium mesh was adequate.

Figs. 11-16 compare computed surface pressures with those from the wind tunnel test at 9 stations on the model for two angles-of-attack for the three grids. The main features of forebody and wing leading-edge vortices are captured, and the overall Cp levels show reasonable agreement throughout, i.e., reasonable enough for preliminary design purposes. In Fig. 11, the double peak near the chine at Stations 2 and 3 is a numerical overshoot, and not evidence of a secondary vortex. In general, refining the grid increases the vortex suction peaks as expected.

The analysis with wind tunnel walls present was performed by truncating the outer cartesian gridblock and adding a new block extending from the tunnel walls inward to overlap the outer block. The afterbody/sting block was cut off, and a cap placed over the end above the tunnel floor (Fig. 17). Fig. 18 shows a front view of the overlap arrangement. Fig. 19 compares the results of free air and wind tunnel wall calculations with the test data corrected for sting and wall interference. At 10 deg., the wall effects are minimal, which is in agreement with data. Conclusions are more difficult for the high alpha case since the calculations are unsteady.

The variations in surface pressures at 10 deg. due to walls are shown in Figs. 20, 21. Considering how closely forces and moments match each other at this alpha, one would not expect surface pressures to be different, however, the solution with walls present was not advanced as far as the one without walls. This could be why the details of the Cp curves do not match precisely. The 35 deg. case variations (Figs. 22, 23) could reflect the flow unsteadiness. Tunnel non-uniformities (if any) are also not being modeled, nor is the precise sting geometry present. Insufficient time prevented a more careful study.

3.2 Computational Matrix

The main computational matrix consisted of 22 runs of the various geometries in alpha and sideslip sweeps. The grid generation, execution, and postprocessing of these runs was completed in about 8 weeks. The results were broken down into three groups for comparison: the effect of forebody chine angle, the effect of vertical tail configuration, and the effect of sideslip angle.

Fig. 24 summarizes the force and moment variations with angle-of-attack for the 100-deg. chine angle (MTVI1) and the 30-deg. chine angle (MTVI3). The sharp chine shows increased lift and moment due to the more powerful forebody vortex it generates. $C_{L_{max}}$ is also higher, in agreement with data. Figs. 25 and 26 compare contours of total pressure at several stations down the body. Lower total pressure for the sharp chine indicates a more concentrated vortex. Particle trace patterns for these cases give further indications of changes in the forebody flowfield (Figs. 27, 28). Particles were released from the chine, the wing leading-edge, and from the forebody vortex core. For the 100-deg. chine, the flow emanating from the forebody leading-edge is split between the forebody vortex and the wing leading-edge vortex. The flow of the 30-deg. chine case, on the other hand, is dominated by the forebody vortex. Surface pressure comparisons (Figs. 29, 30) indicate higher forebody vortex suction peaks for the sharp chine geometry and lower Cp's at the wing leading-edge vortex.

Results summarizing the effect of vertical tail configuration are plotted in Fig. 31. The twin tails over the wing case (MTVI1) is compared to a single vertical tail on the aftbody centerline (MTVI2). The increased lift, decreased drag, and decreased pitching moment of the single tail geometry are all predicted by the calculations. Also, the different character of the force and moment curve breaks at $C_{L_{max}}$ are reproduced remarkably well by the Euler results. Upper surface Mach number contours for these two cases at 22.5 deg. angle-of-attack (Figs. 32, 33) show that the twin vertical configuration destroys the vortex system over the wing and separates the flow outboard of the vertical tail. The particle traces in Fig. 34 show a coherent vortex system over the single tail geometry wing, whereas the forebody and leading-edge vortices are interrupted by the twin tail, causing a loss in lift (Fig. 35). This could cause the more gradual stall indicated by the twin tail lift curve rather than the sharp stall of the single tail case, which would be driven by the wing vortex bursting. The surface pressure comparison (Figs. 36, 37) shows evidence of the stronger wing leading-edge vortex.

The effect of sideslip angle was examined by comparing the single and twin tail configurations with the 100 deg. forebody chine angle at sideslip (beta) angles of up to 6 deg. The lower righthand plot of Fig. 31 shows yawing moment as a function of beta for these cases at alpha = 30 deg. Considering that the longitudinal forces and moments agree with data so well for these configurations, as well as the surface pressures, the magnitudes of yawing moment should be in better agreement. One problem with OVERFLOW is that it currently has no built-in force and moment reduction capability. It simply puts out an array of three-axis force and moment numbers it assigns to each segment in each block tagged as surface points. After the run, these numbers must be summed, renormalized, and transformed into the appropriate axis system. Another problem is that since this is an overset mesh method, some surface point segments may overlap, so a certain amount of guesswork and editing is necessary to insure that the surface of the configuration is covered only once. It is quite possible that the yawing moment coefficient was reduced incorrectly, and there was insufficient time to investigate and correct it. However, the increased effectiveness of the single tail configuration in yaw is predicted correctly. At higher sideslip angles (beta = 6 deg.) the effectiveness is about the same as the twin tail case, which is also in agreement with test data.

Figs. 38 and 39 compare particle traces for the 0 deg. and 6 deg. runs of the single tail configuration. In sideslip, the windward vortex (left) moves closer to the body and the leeward vortex moves further away. In Fig. 40, it can also be seen that the windward vortex burst point moves forward. Surface pressure comparisons for the two configurations at 22.5 deg. angle-of-attack (Figs. 41-44) confirm the vortex movement and burst shown in the previous figures. Fig. 42, Station 6, shows a flattening of the Cp curve on the right side of the configuration at beta = 6, as opposed to the distinctive double peak of the two vortex flow at beta = 0, indicating windward vortex burst. The calculation agreement with test data, for the single tail geometry case in particular, is remarkable.

Two final runs were made for the twin tail geometry with undeflected leading-edge flap at the angles-of-attack of the pathfinder study. Although not plotted here, a small increase in lift occurred at alpha = 10 deg., and no change in lift but decreased pitching moment resulted at 35 deg.

4.0 CONCLUSIONS

State-of-the-art Euler analysis methods, of which OVERFLOW-Chimera is but one example, can be applied to complex aircraft configurations for the purpose of extracting information useful to preliminary design in a timely fashion (1-2 weeks). This study shows that force and moment predictions for configurations of this type are of sufficient accuracy through $C_{L_{max}}$ to assess major design options. The principal flow phenomena present in vortical flows over sharp-edge geometries are captured. Early insight into complex aerodynamic effects are also provided by the detailed flowfield information available from Euler analysis.

Further study based on this investigation should include a more careful evaluation of this configuration at specific conditions of interest for the purpose of identifying flowfield cause and effect relationships. This explanatory process is often a key factor in preliminary design. Another suggestion is to investigate the physical modelling aspects of Euler methods with respect to vortex burst.

5.0 REFERENCES

1. Buning, P.G., Chan, W.M., Renze, K.J., Sondak, D.L., Chiu, I.T., and Slotnick, J.P., "OVERFLOW User's Manual, Version 1.6ab," NASA Ames Research Center, Moffett Field, CA, January, 1993.

2. Steinbrenner, J.P., Chawner, J.R., and Fouts, C.L., "The GRIDGEN 3D Multiple Block Grid Generation System," WRDC-TR-90-3022, July 1990.

3. Benek, J.A., Donegan, T.L., and Suhs, N.E., "Extended Chimera Grid Embedding Scheme with Application to Viscous Flows," AIAA 87-1126-CP, June 1987.

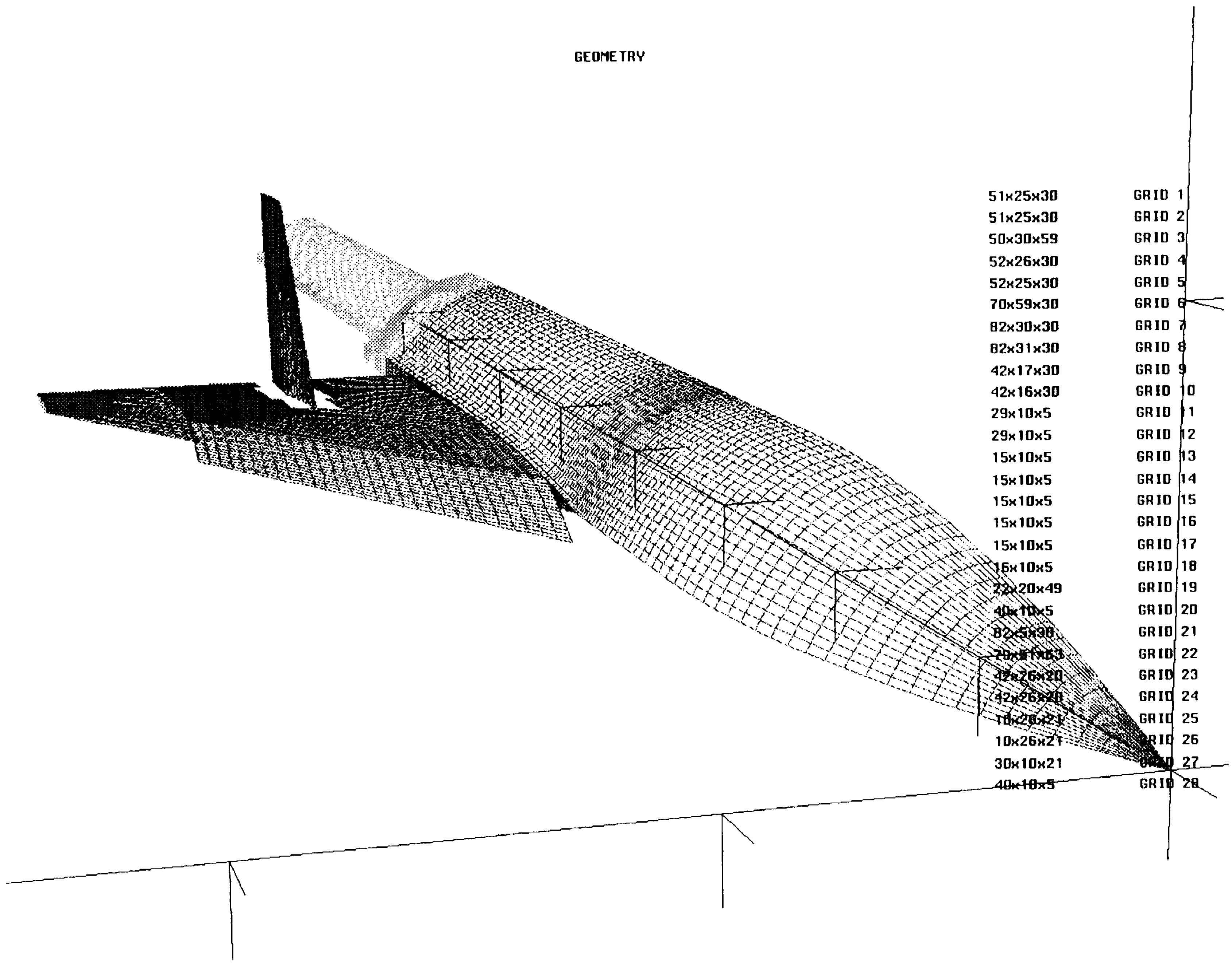

Figure 1. MTVI Surface Grid

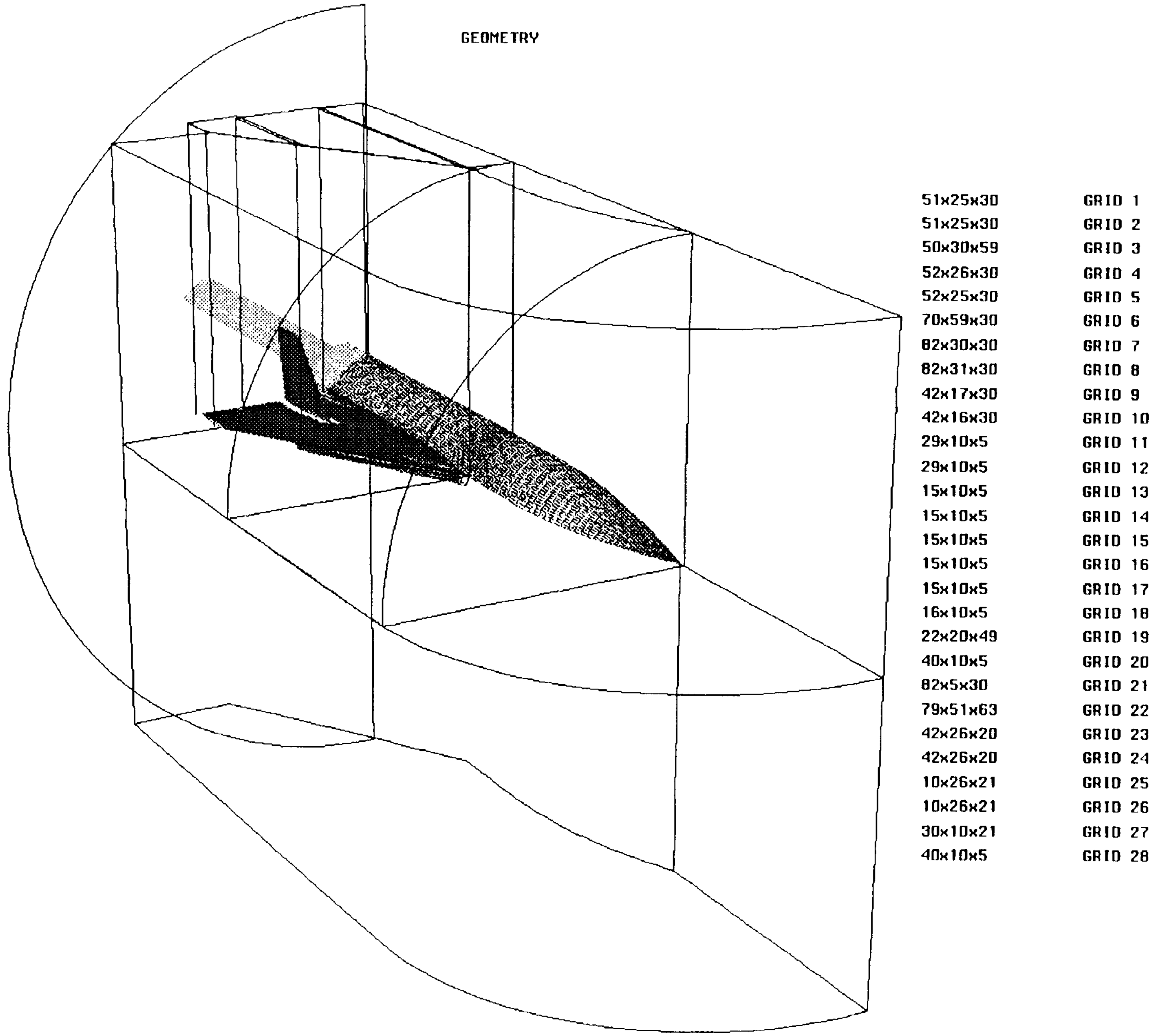

Figure 2. Blocking Scheme

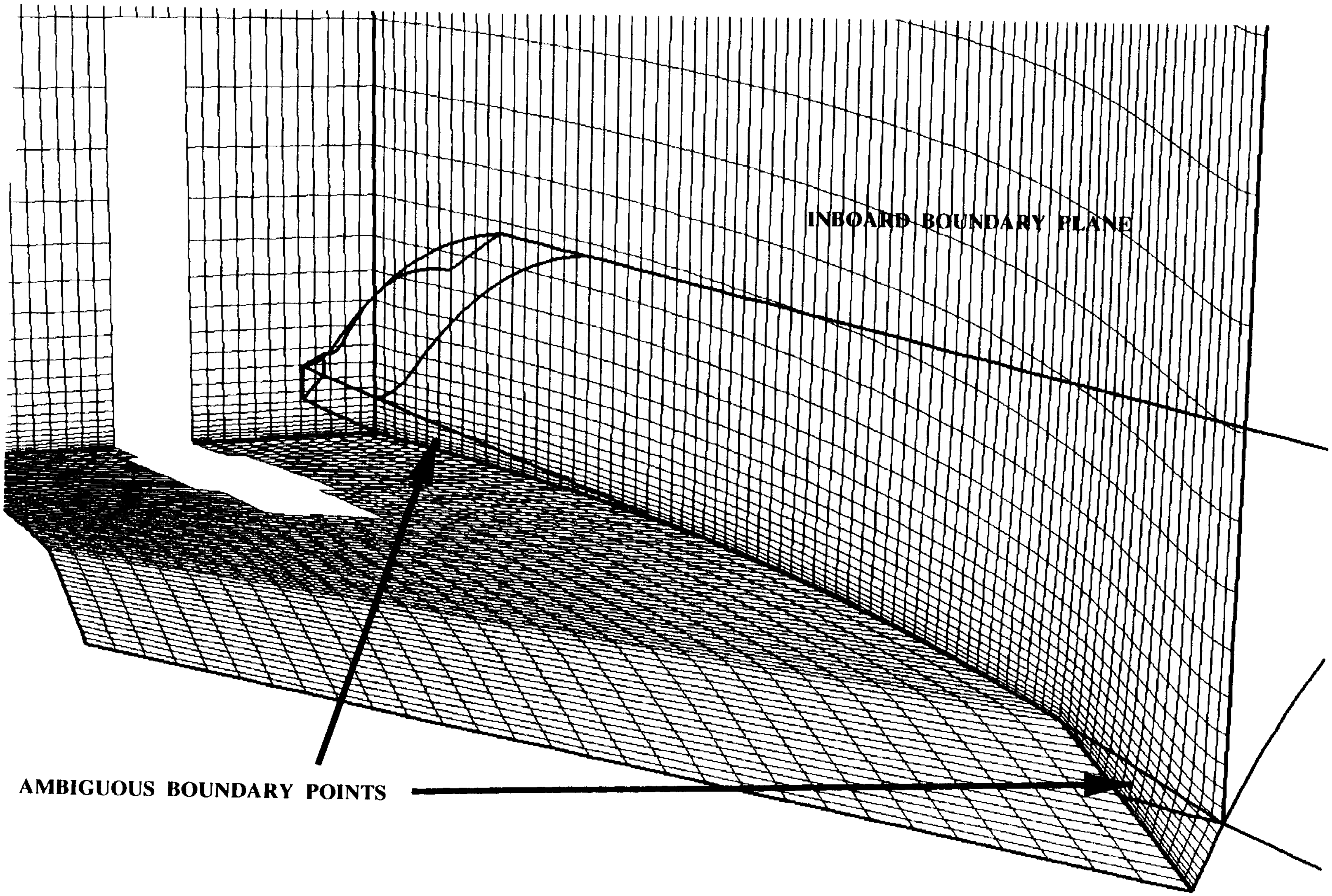

Figure 3. Wing Upper Surface Gridblock

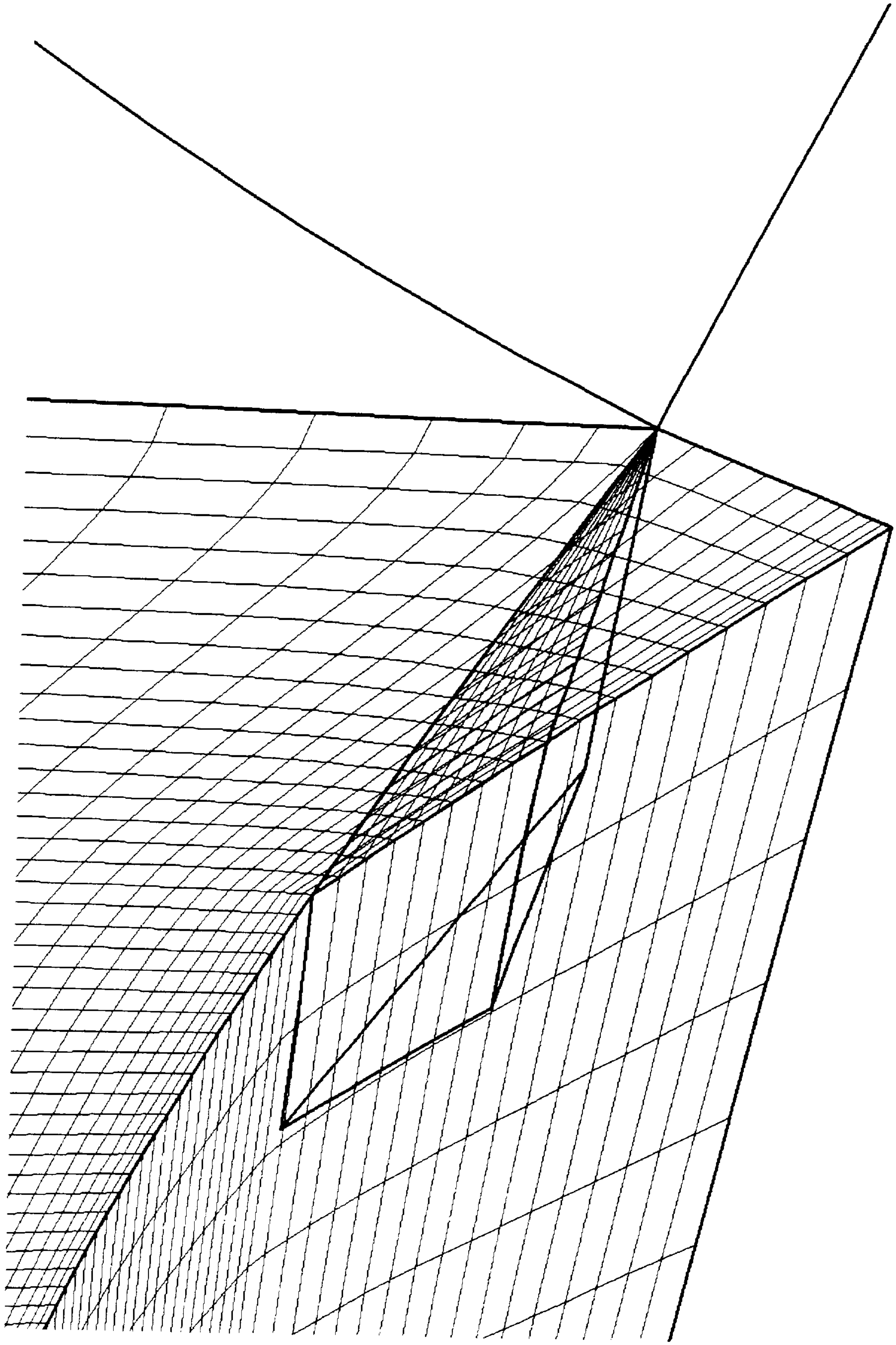

Figure 4. Leading-edge Flap/Body Intersection Region

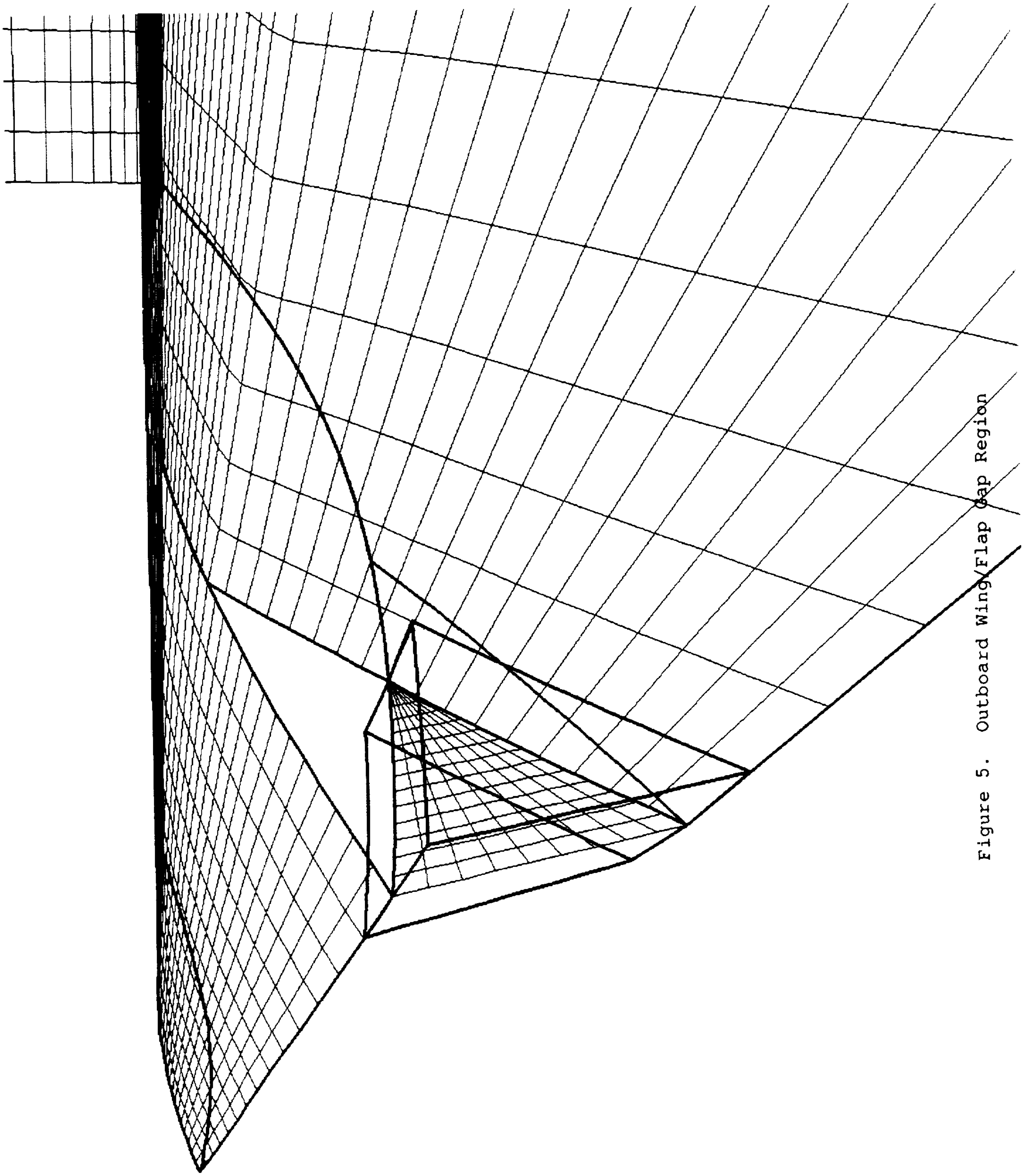

Figure 5. Outboard Wing/Flap Gap Region

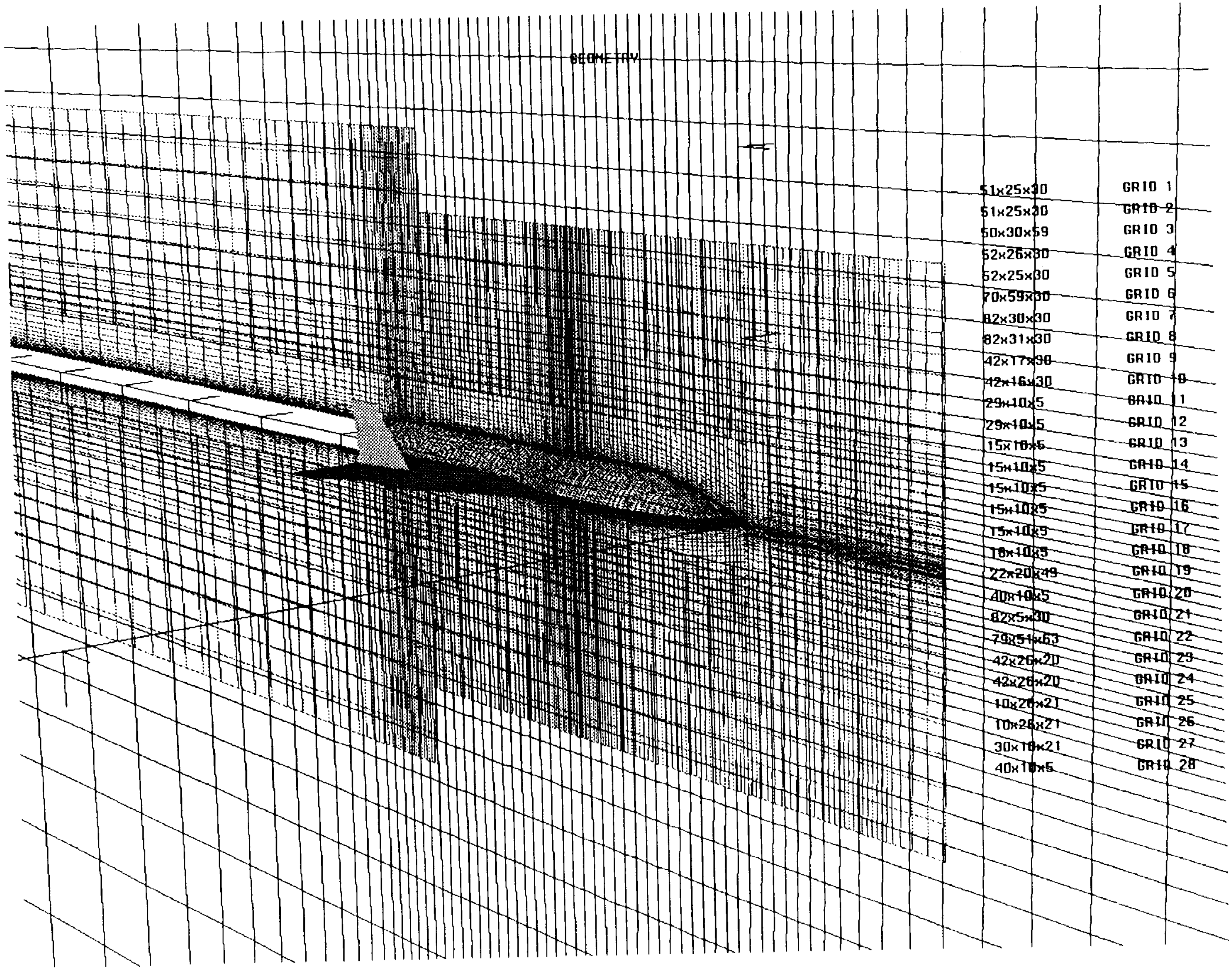

Figure 6. Configuration Centerline Grid

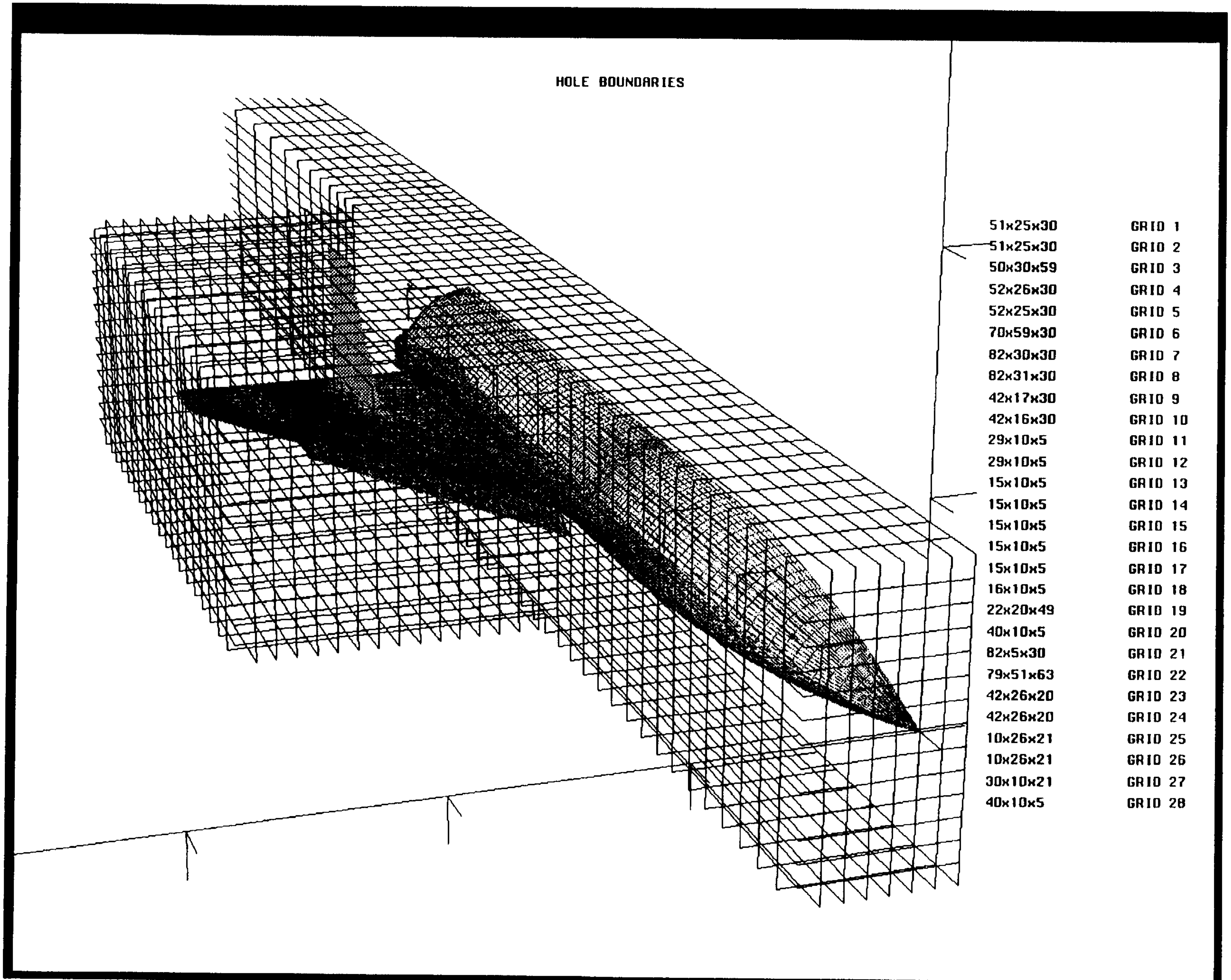

Figure 7. Outer Cartesian Gridblock Hole

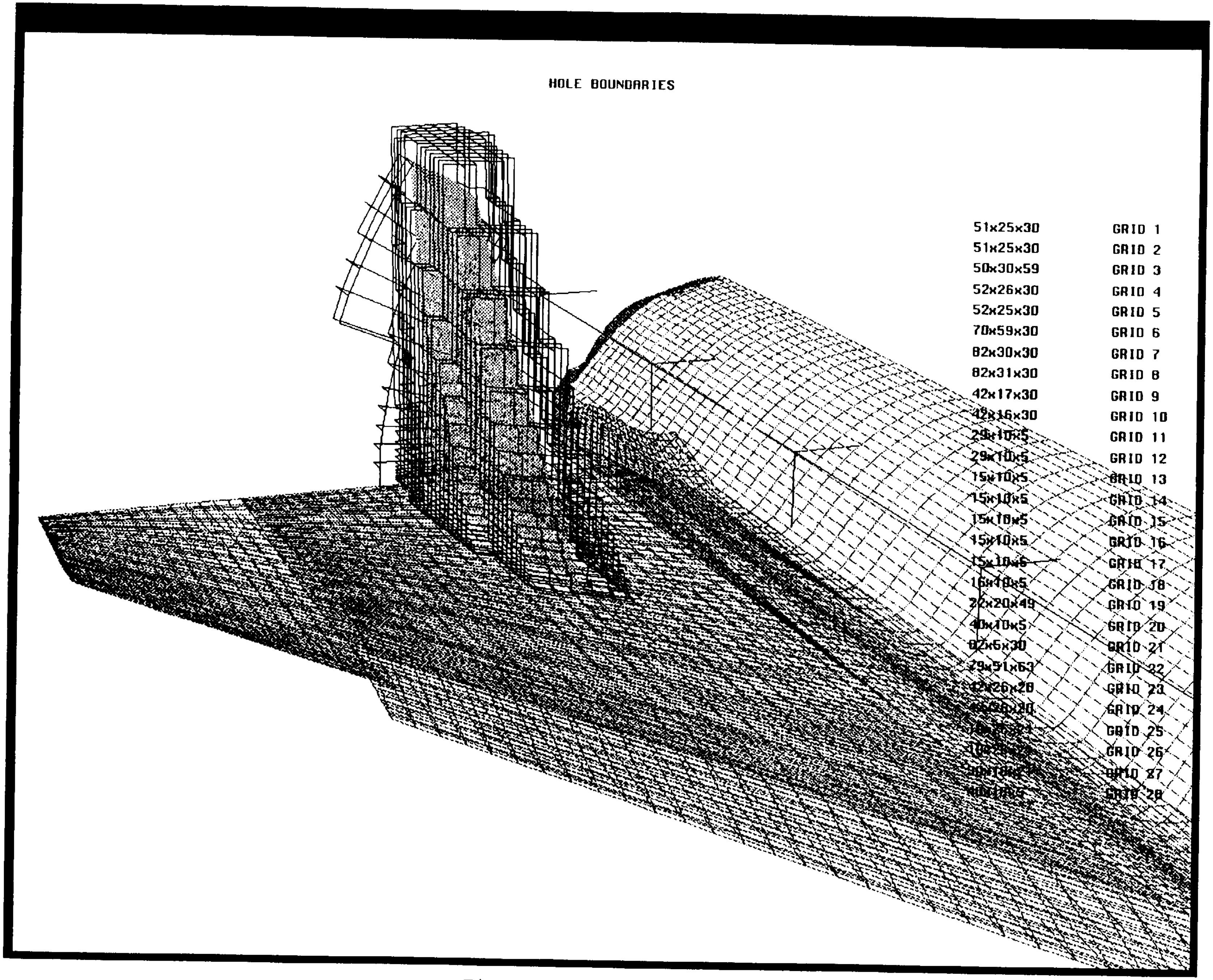

Figure 8. Vertical Tail Hole

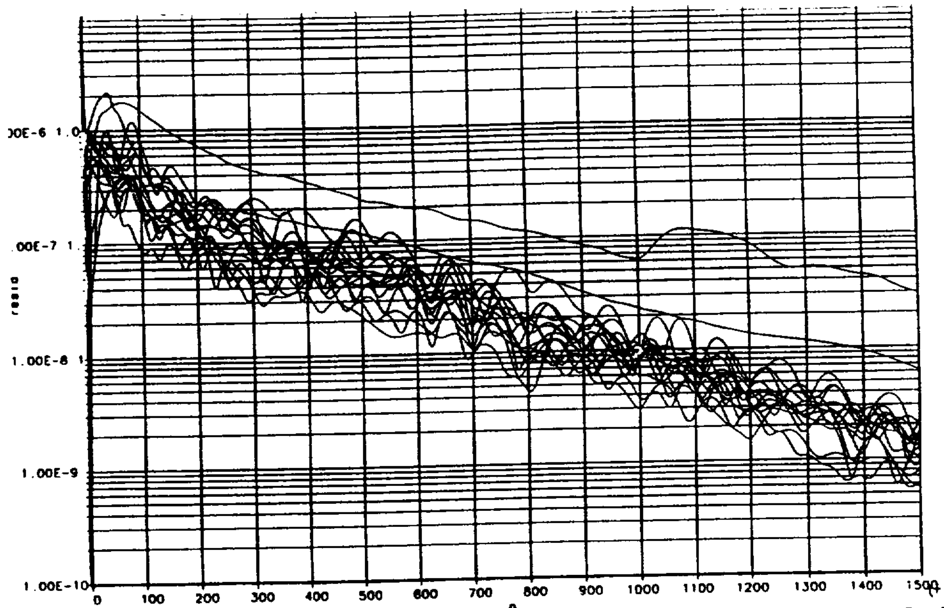

(c). Variation of Lift Coefficient, Medium Mesh, alpha=35.3 deg.

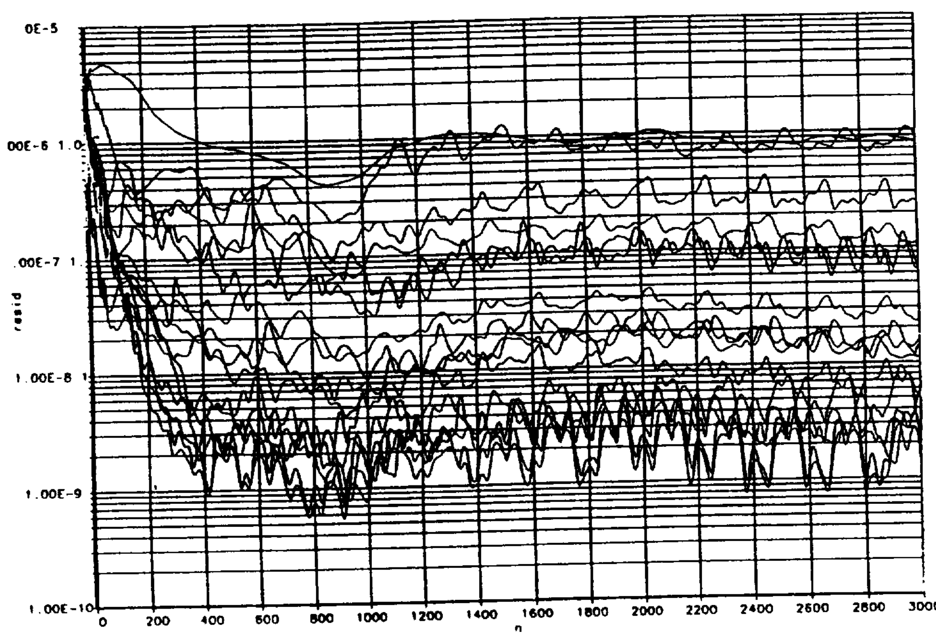

(b). L2-Norm Residual, Medium Mesh, alpha=35.3 deg.

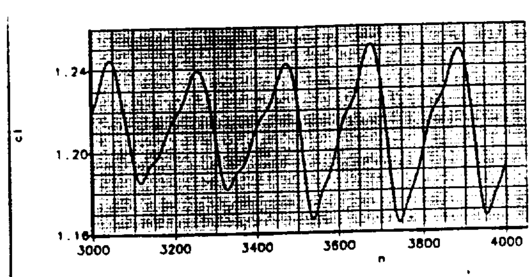

(a). L2-Norm Residual, Coarse Mesh, alpha=10.1 deg.

Figure 9. Convergence Characteristics

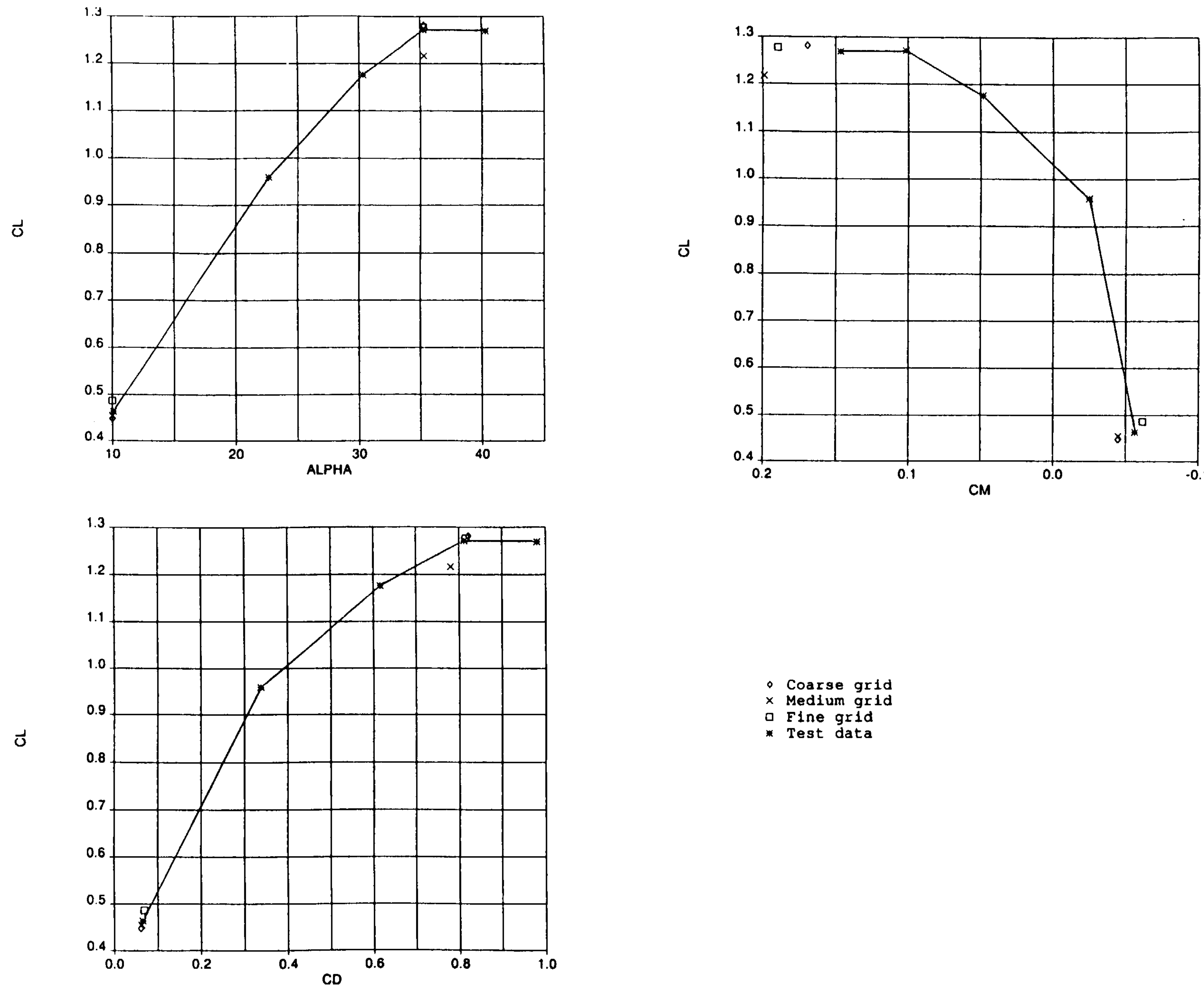

Figure 10. Effect of Grid Refinement

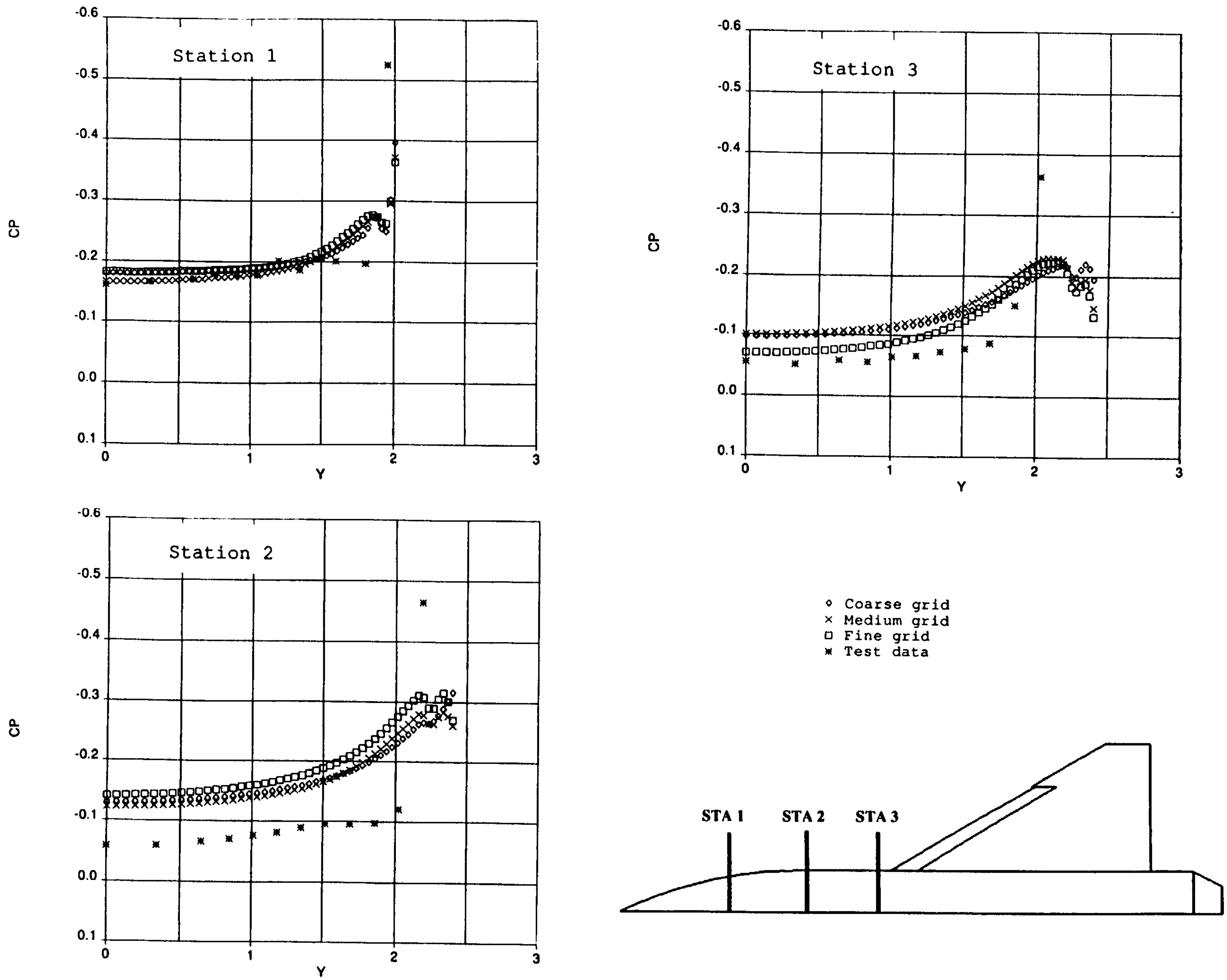

Figure 11. Upper Surface Forebody Pressure Coefficient, MTVI1, alpha=10.1 deg.

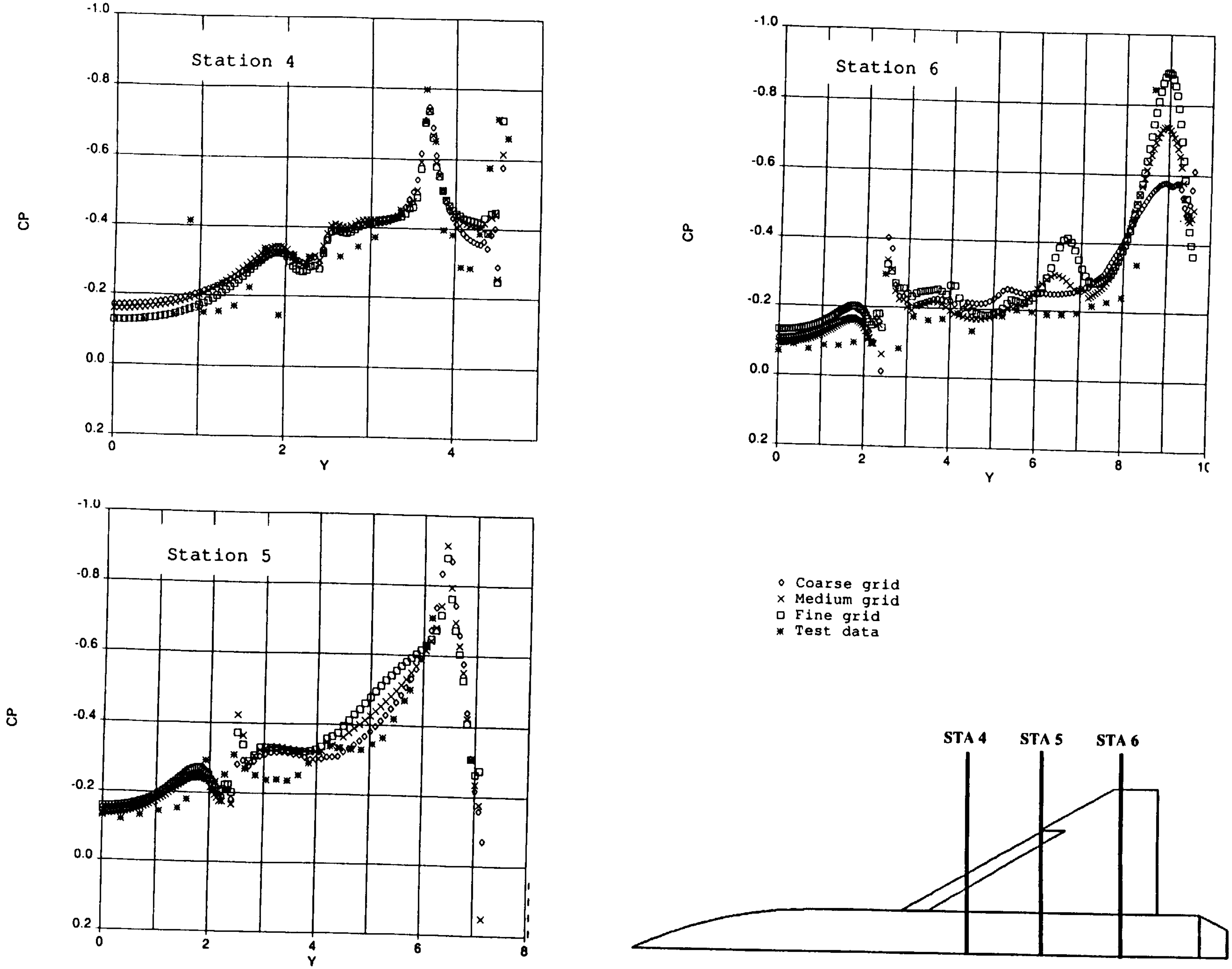

Figure 12. Upper Surface Wing Pressure Coefficient, MTVI1, alpha=10.1 deg.

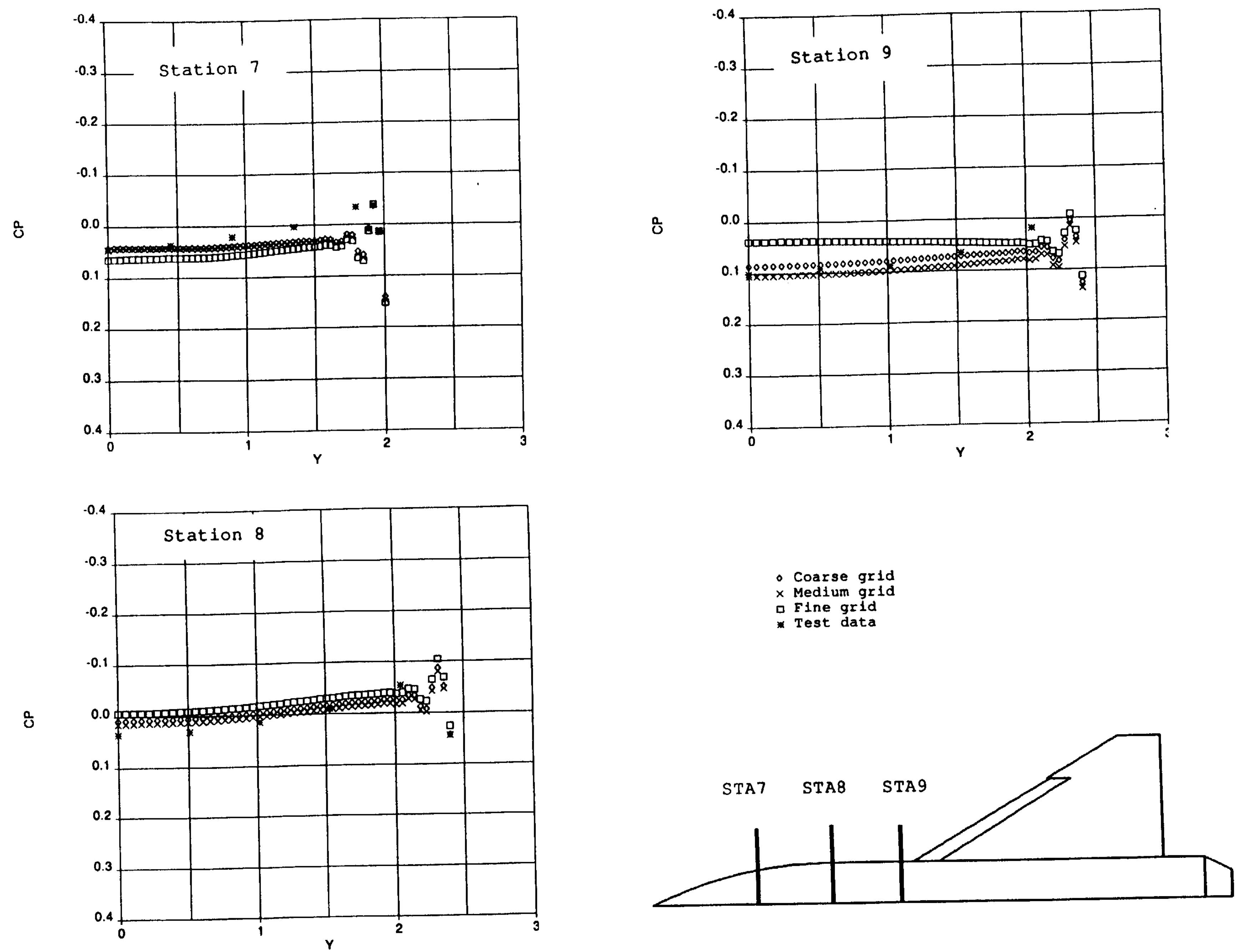

Figure 13. Lower Surface Forebody Pressure Coefficient, MTVI1, alpha=10.1 deg.

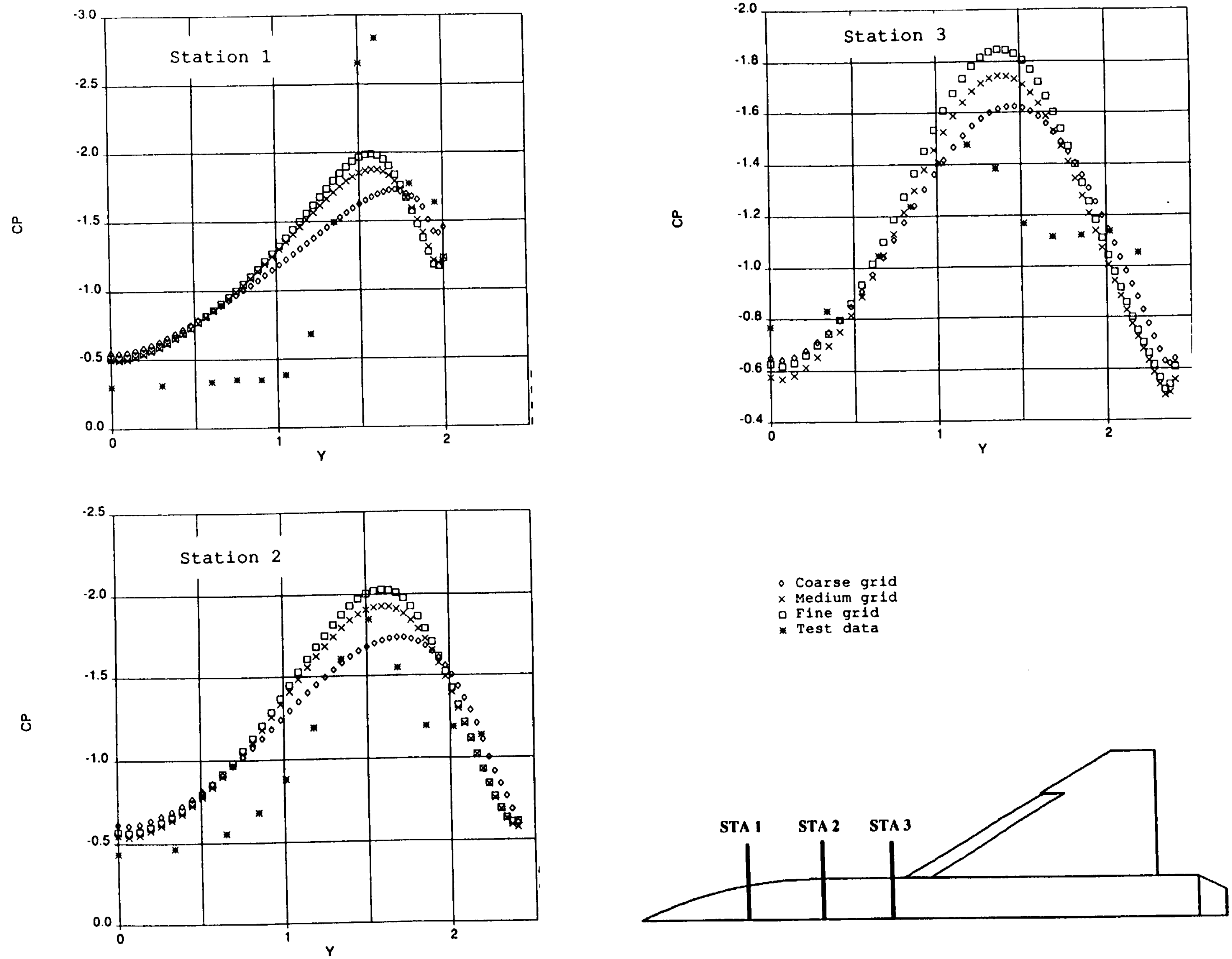

Figure 14. Upper Surface Forebody Pressure Coefficient, MTVI1, alpha=35.3 deg.

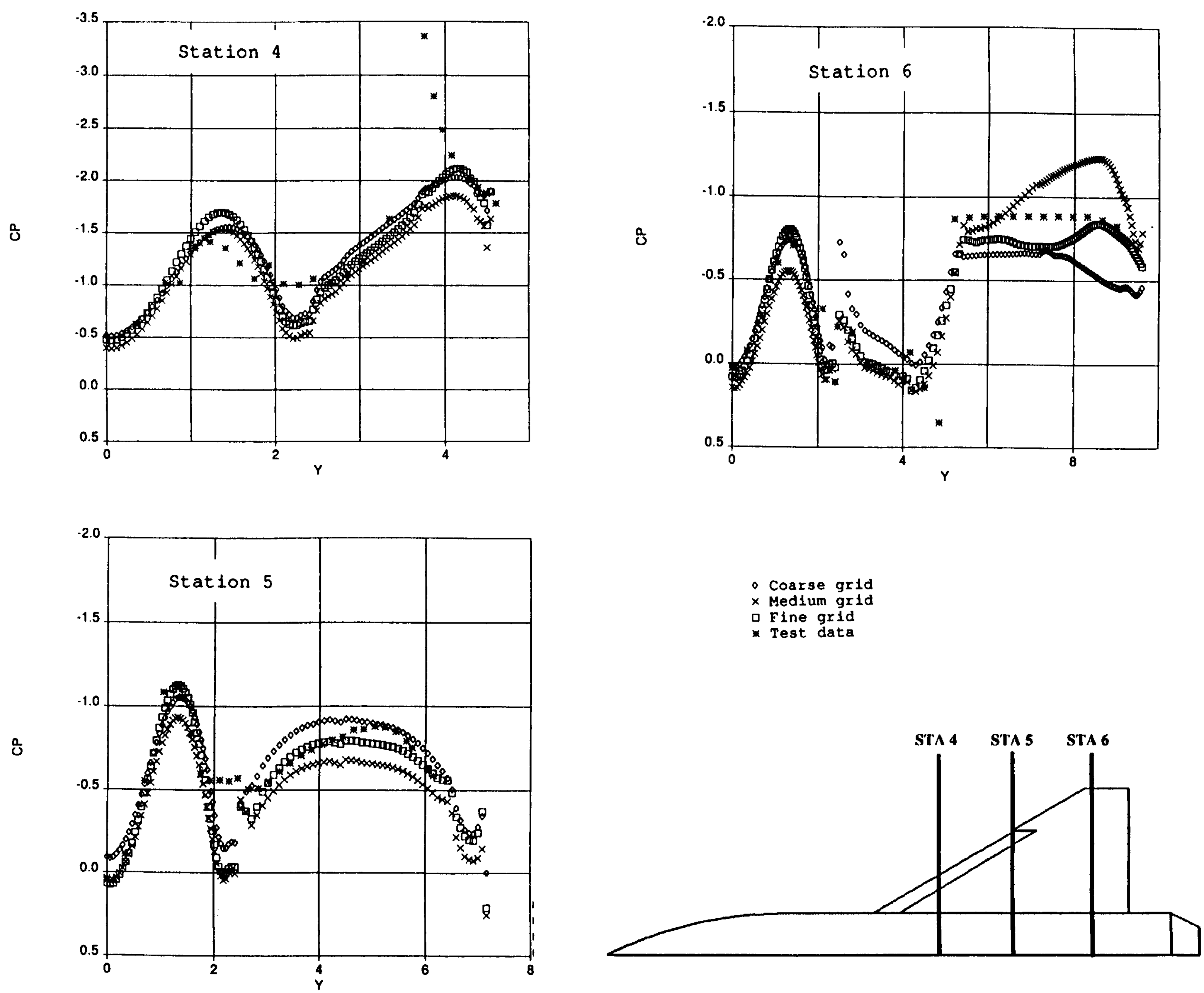

Figure 15. Upper Surface Wing Pressure Coefficient, MTVI1, alpha=35.3 deg.

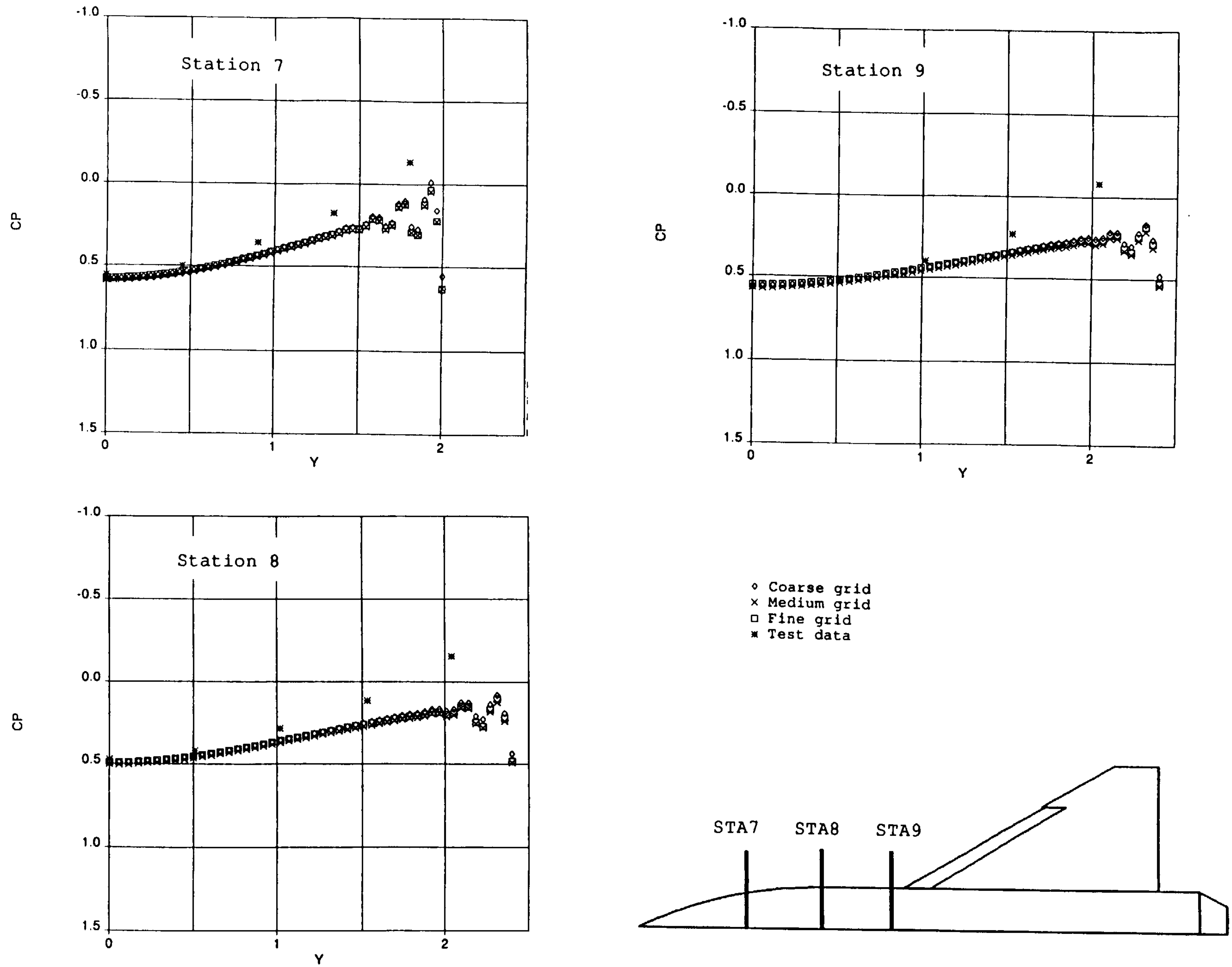

Figure 16. Lower Surface Forebody Pressure Coefficient, MTVI1, alpha=35.3 deg.

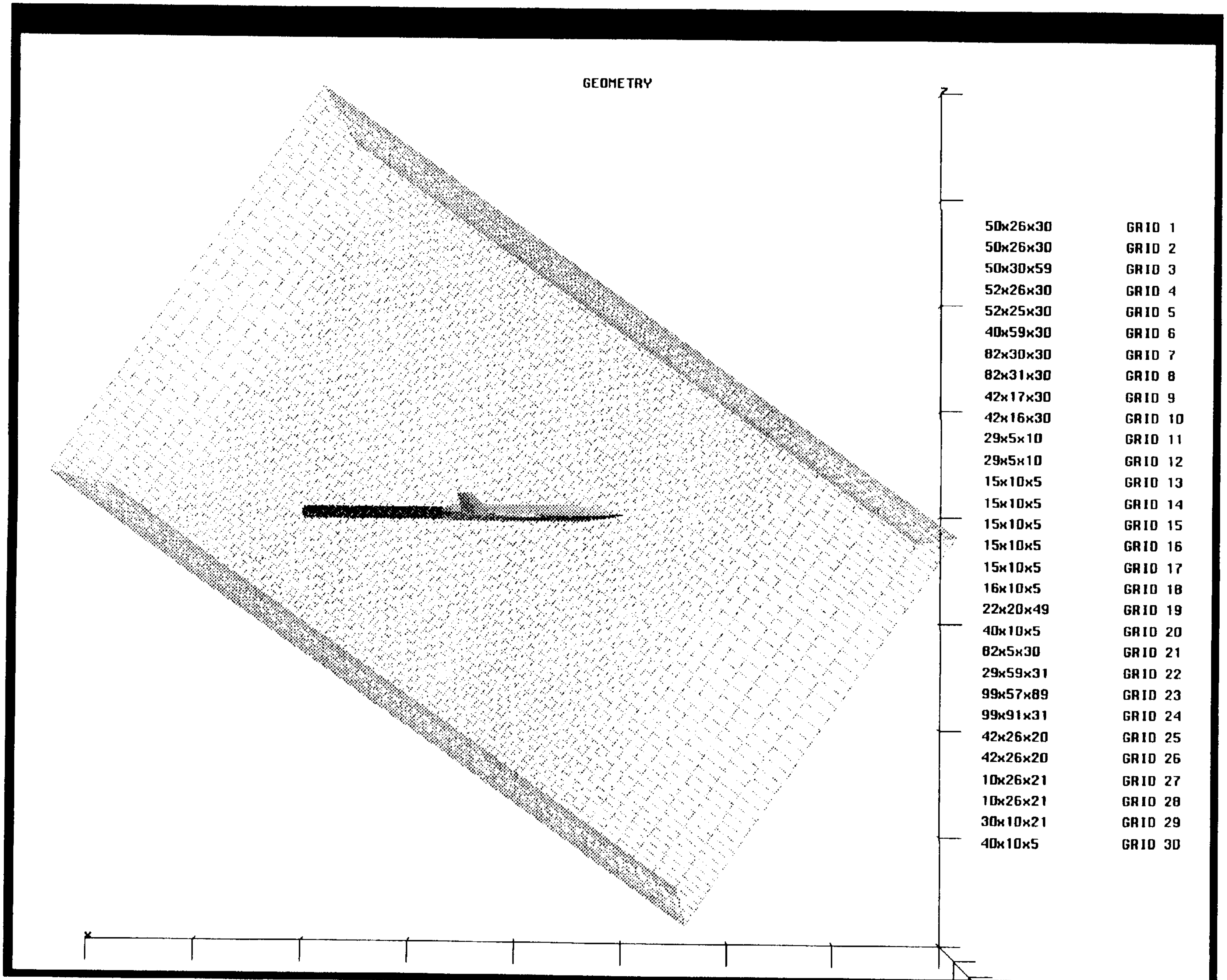

Figure 17. Wind Tunnel Wall Grid, MTVI1, alpha=35.3 deg.

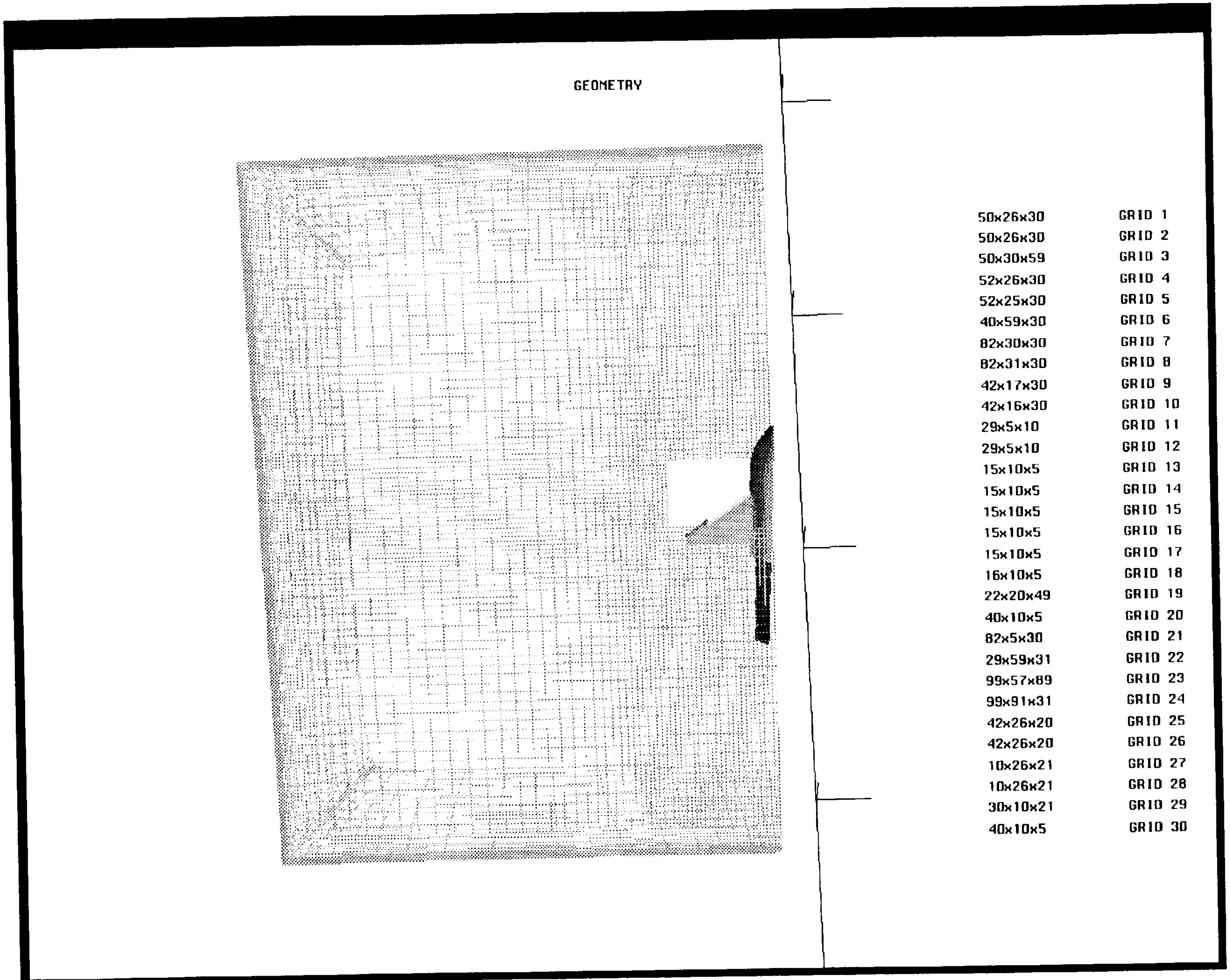

Figure 18. Block Overlap Arrangement, Wind Tunnel Wall Grid

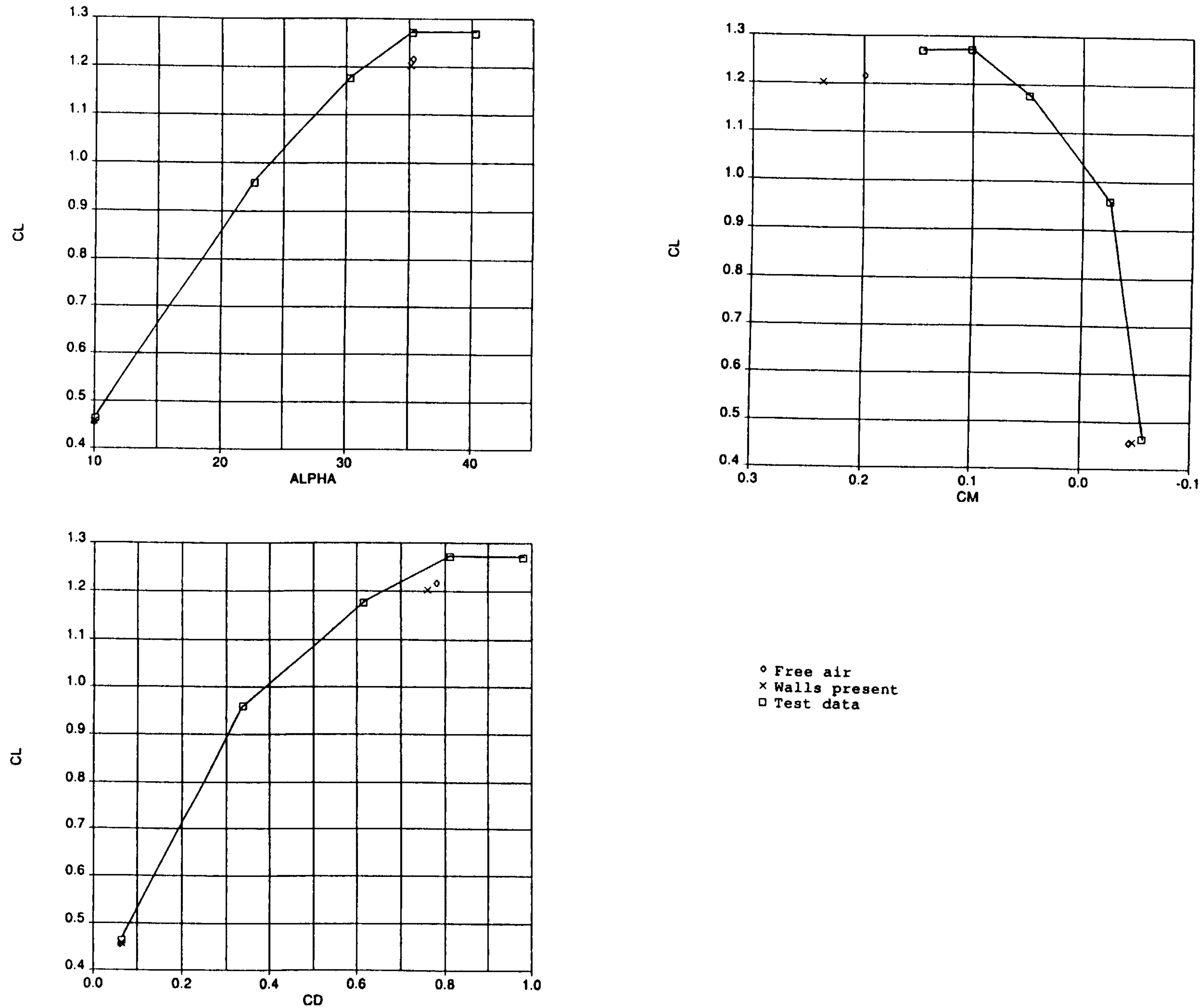

Figure 19. Effect of Wind Tunnel Walls

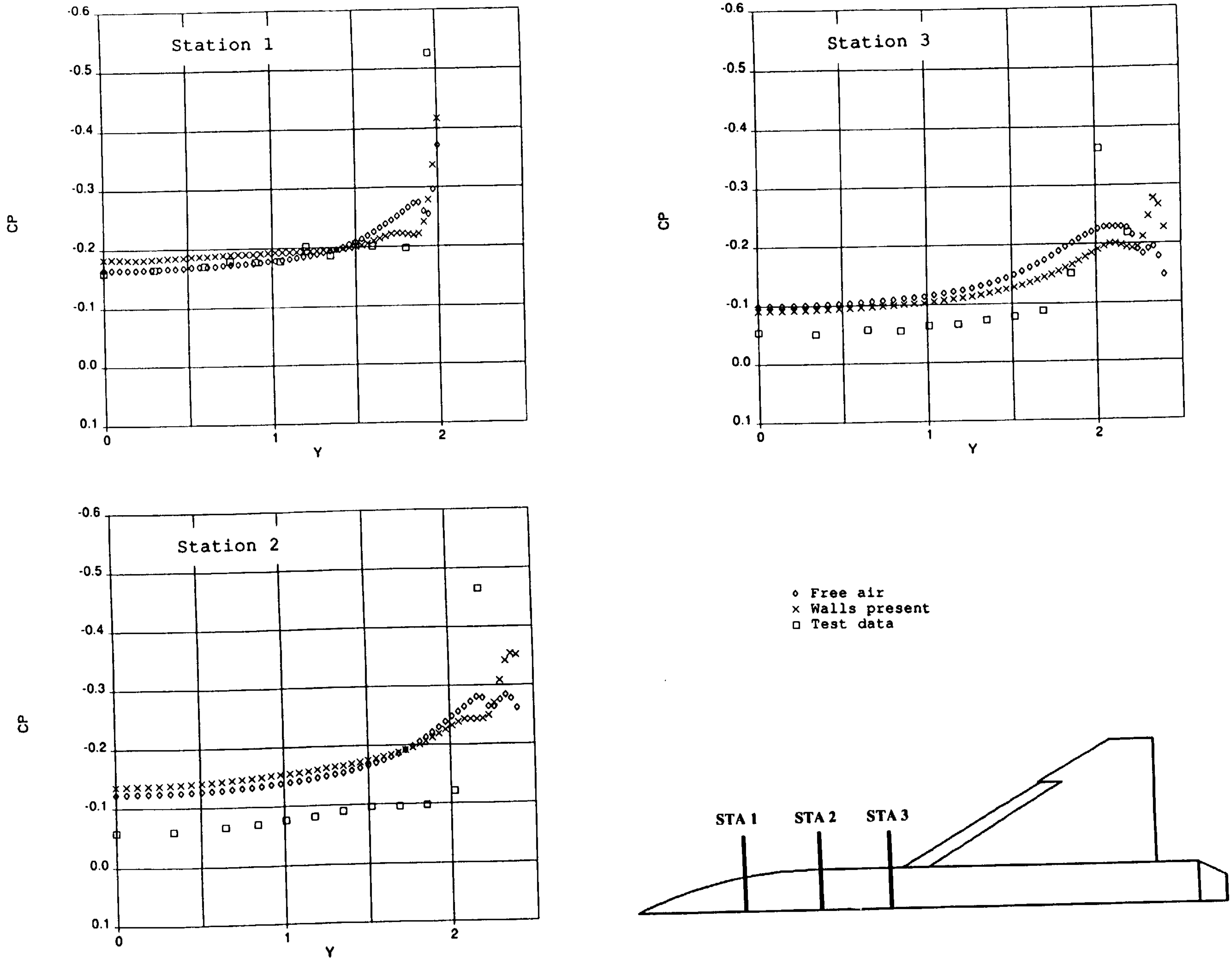

Figure 20. Upper Surface Forebody Pressure Coefficient, MTVI1, alpha=10.1 deg.

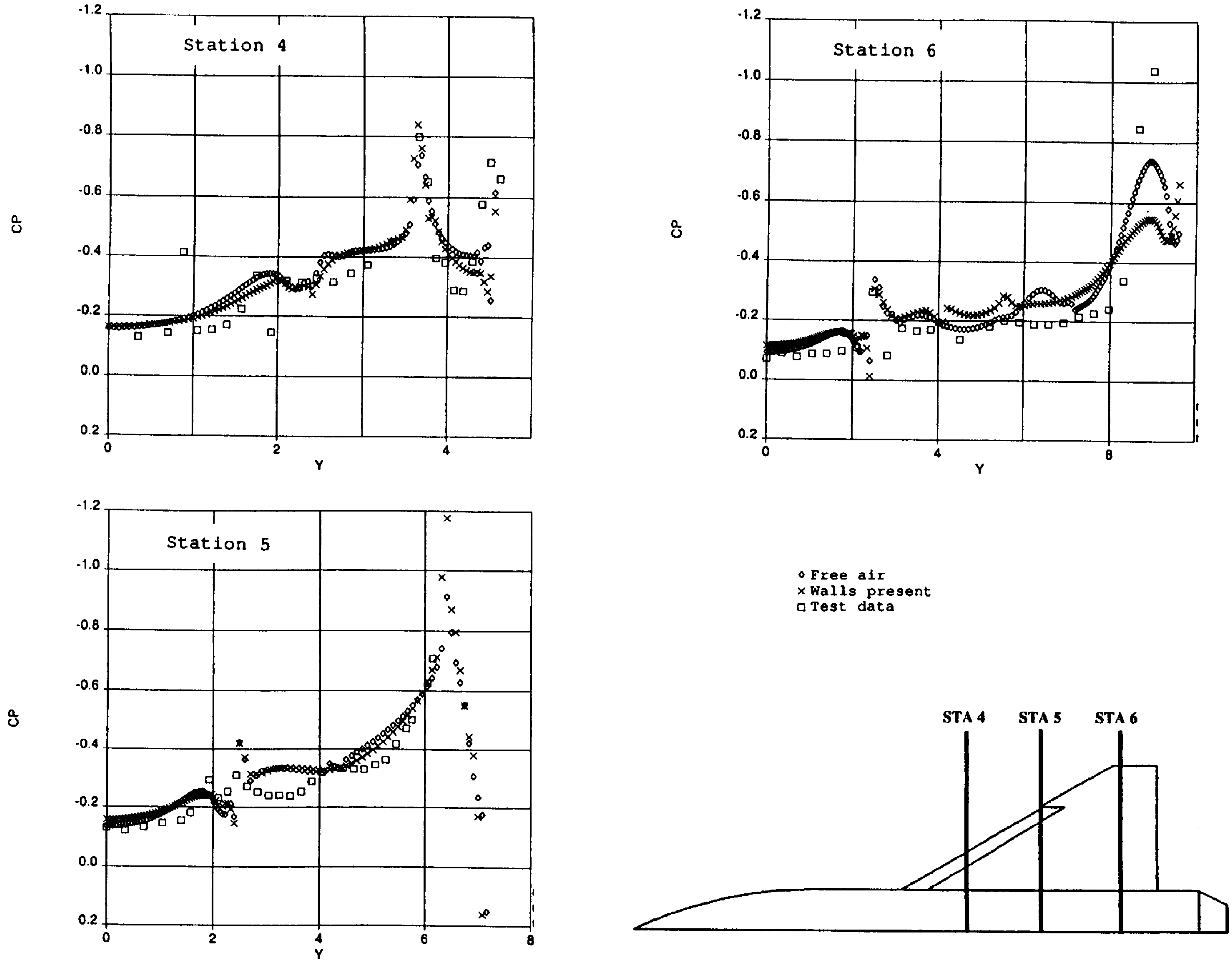

Figure 21. Upper Surface Wing Pressure Coefficient, MTVI1, alpha=10.1 deg.

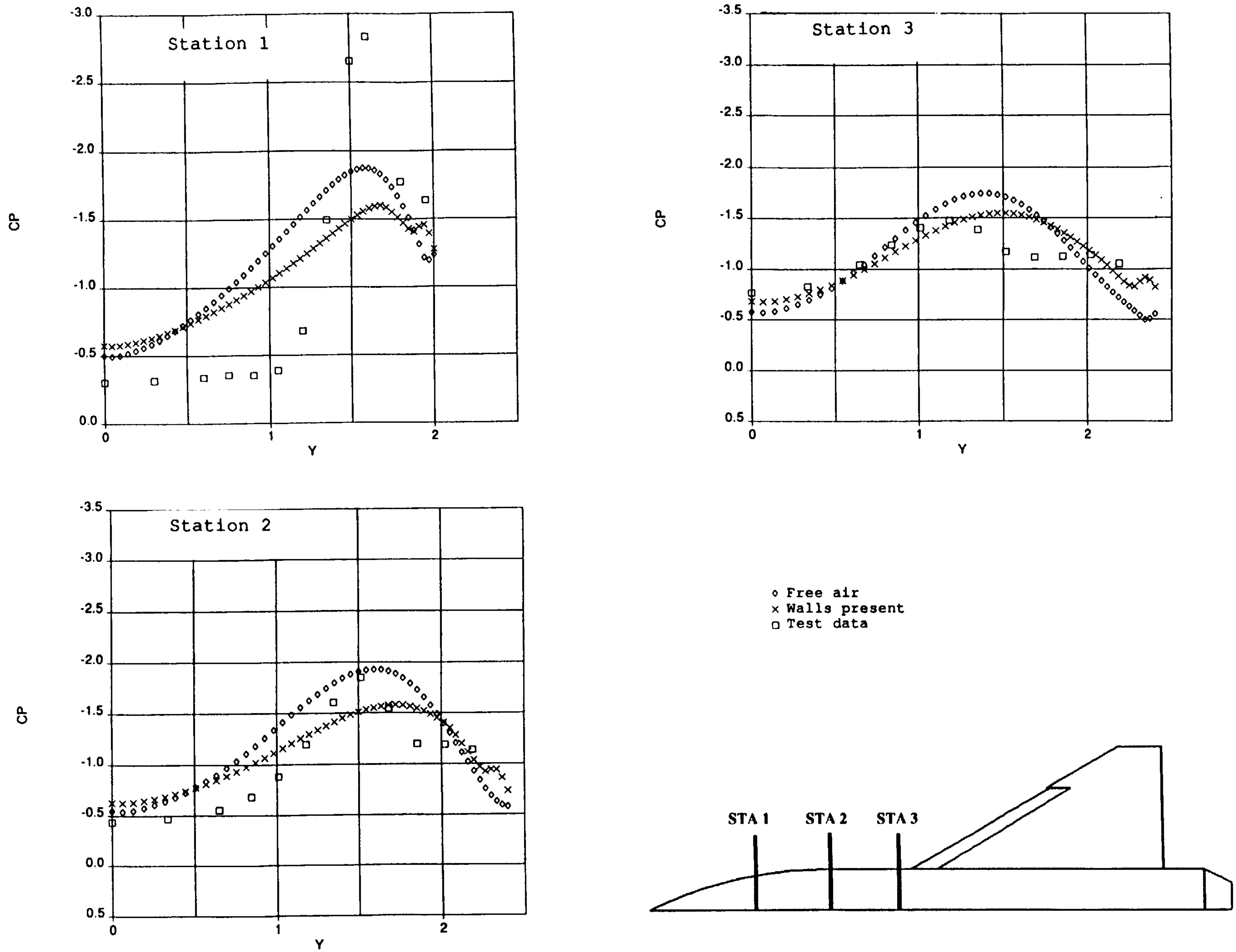

Figure 22. Upper Surface Forebody Pressure Coefficient, MTVI1, alpha=35.3 deg.

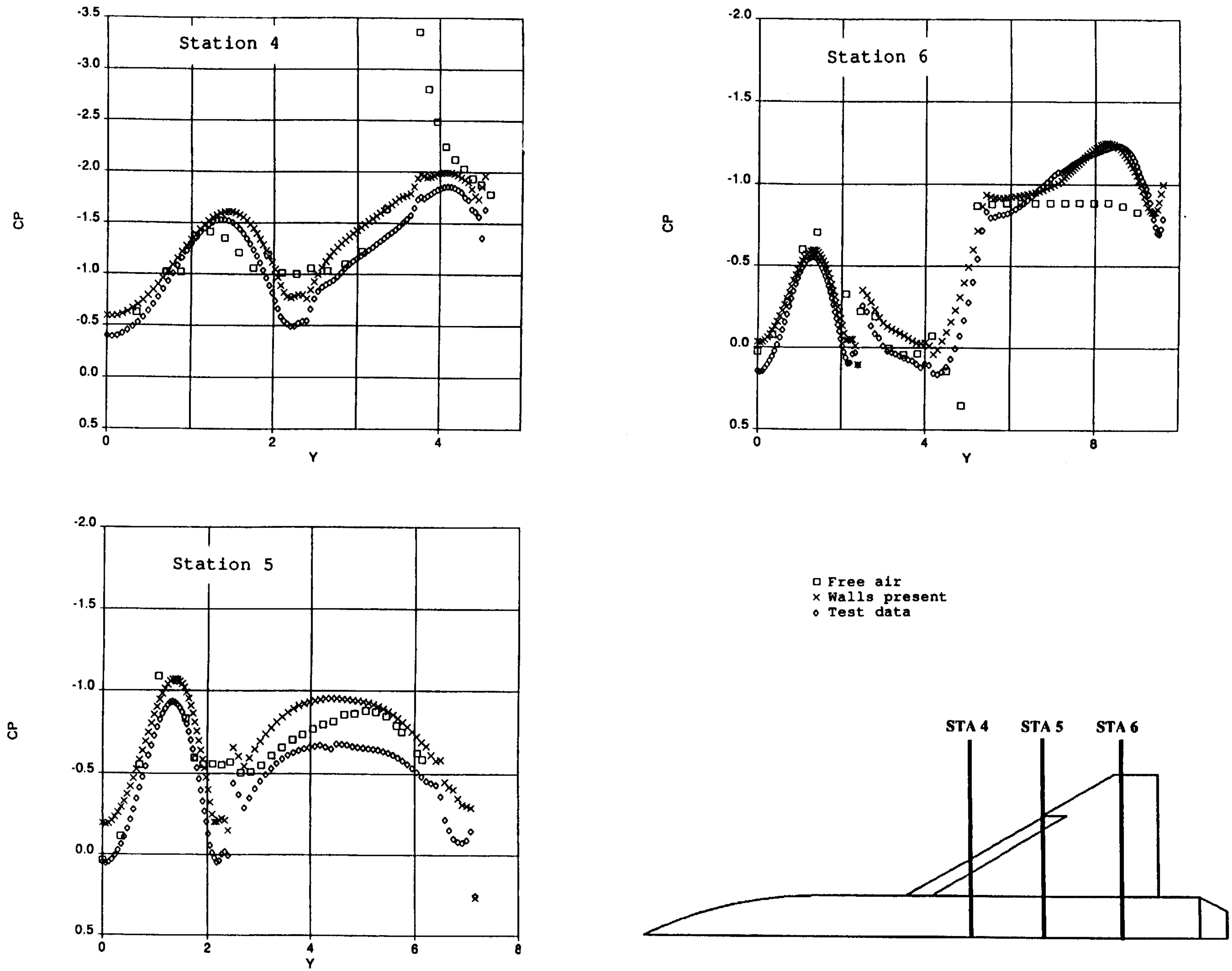

Figure 23. Upper Surface Wing Pressure Coefficient, MTVI1, alpha=35.3 deg.

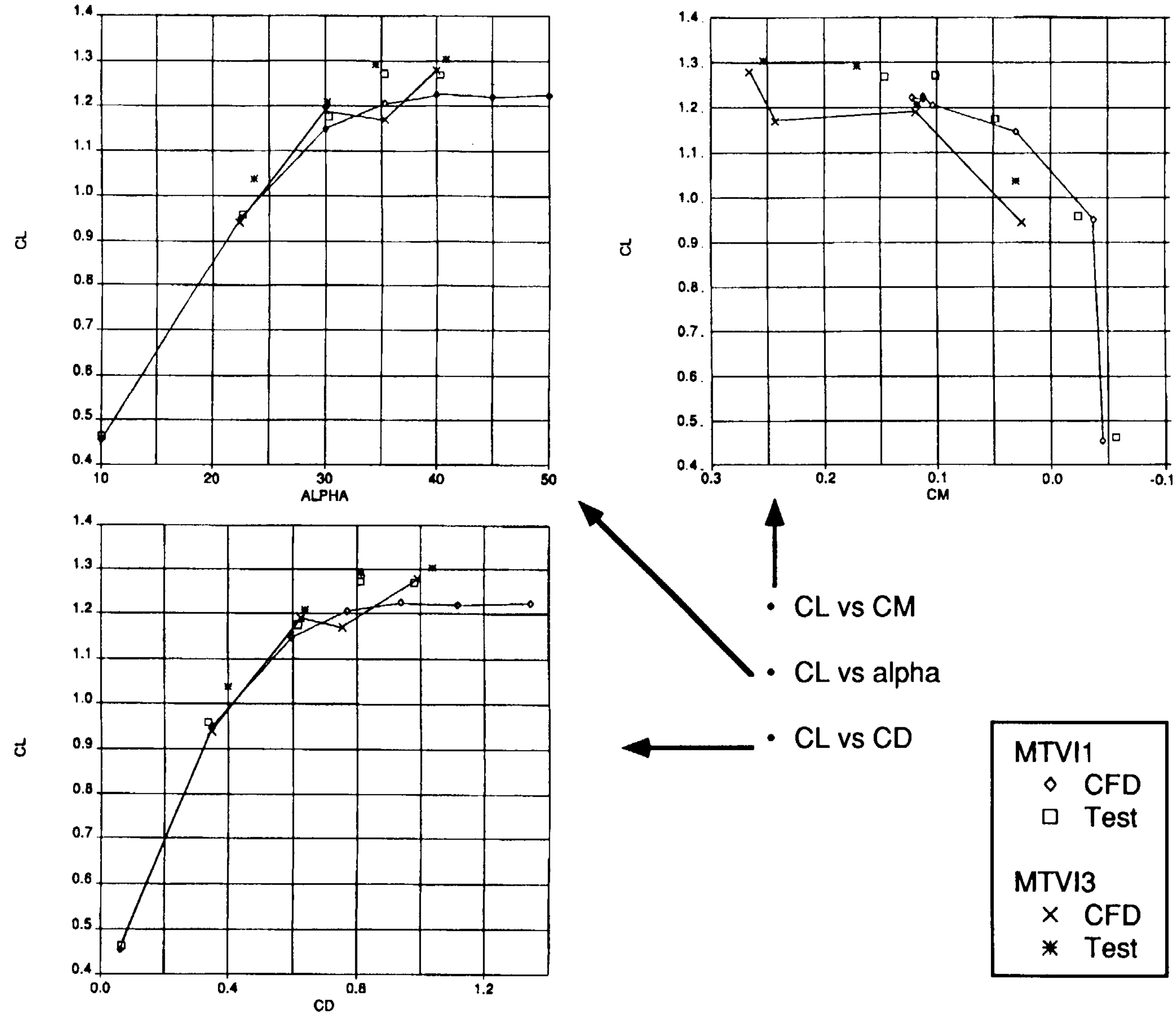

Figure 24. Effect of Chine Angle

spb-8-7-bh-C4a

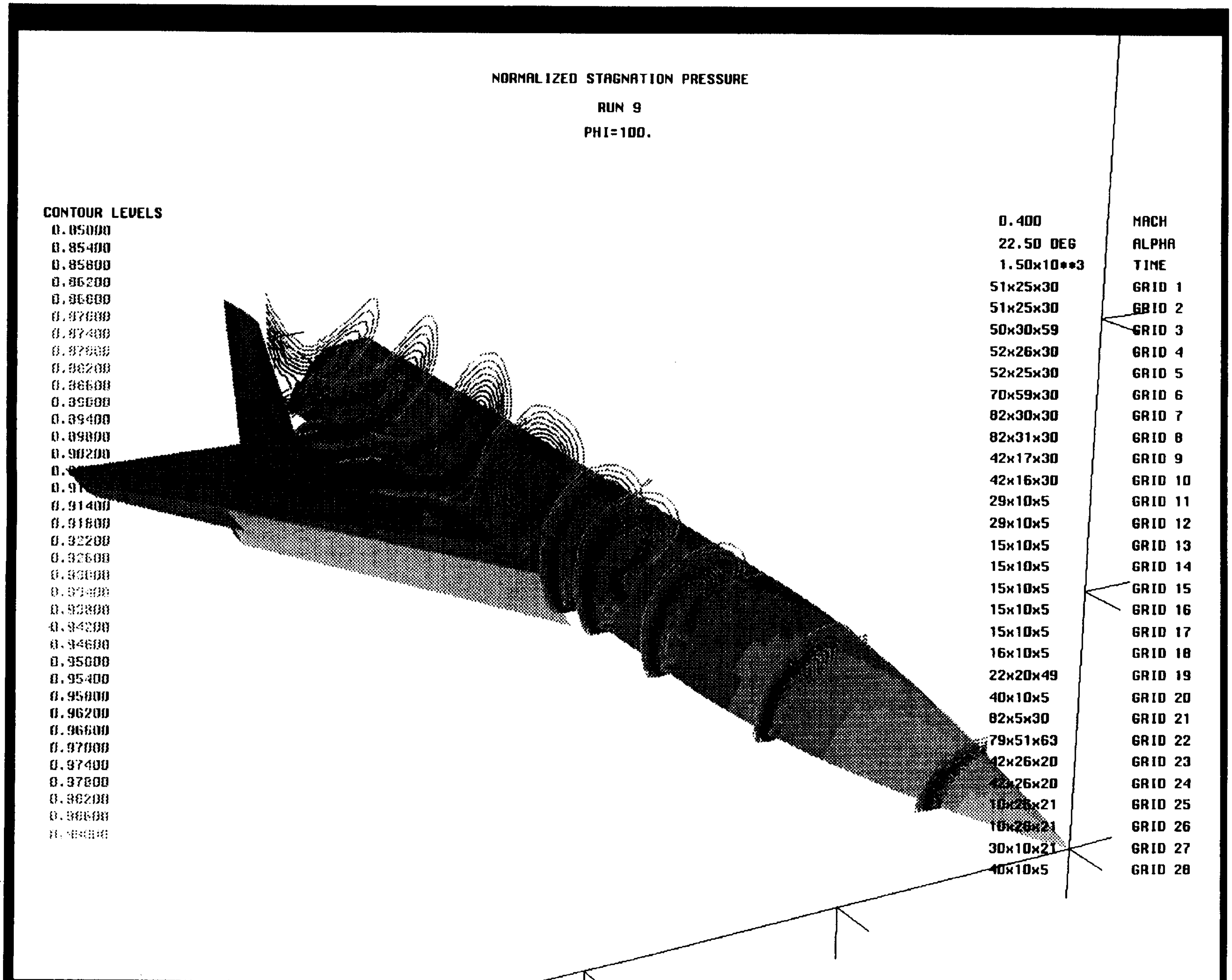

Figure 25. Stagnation Pressure Contours, phi=100 deg., alpha=22.5 deg.

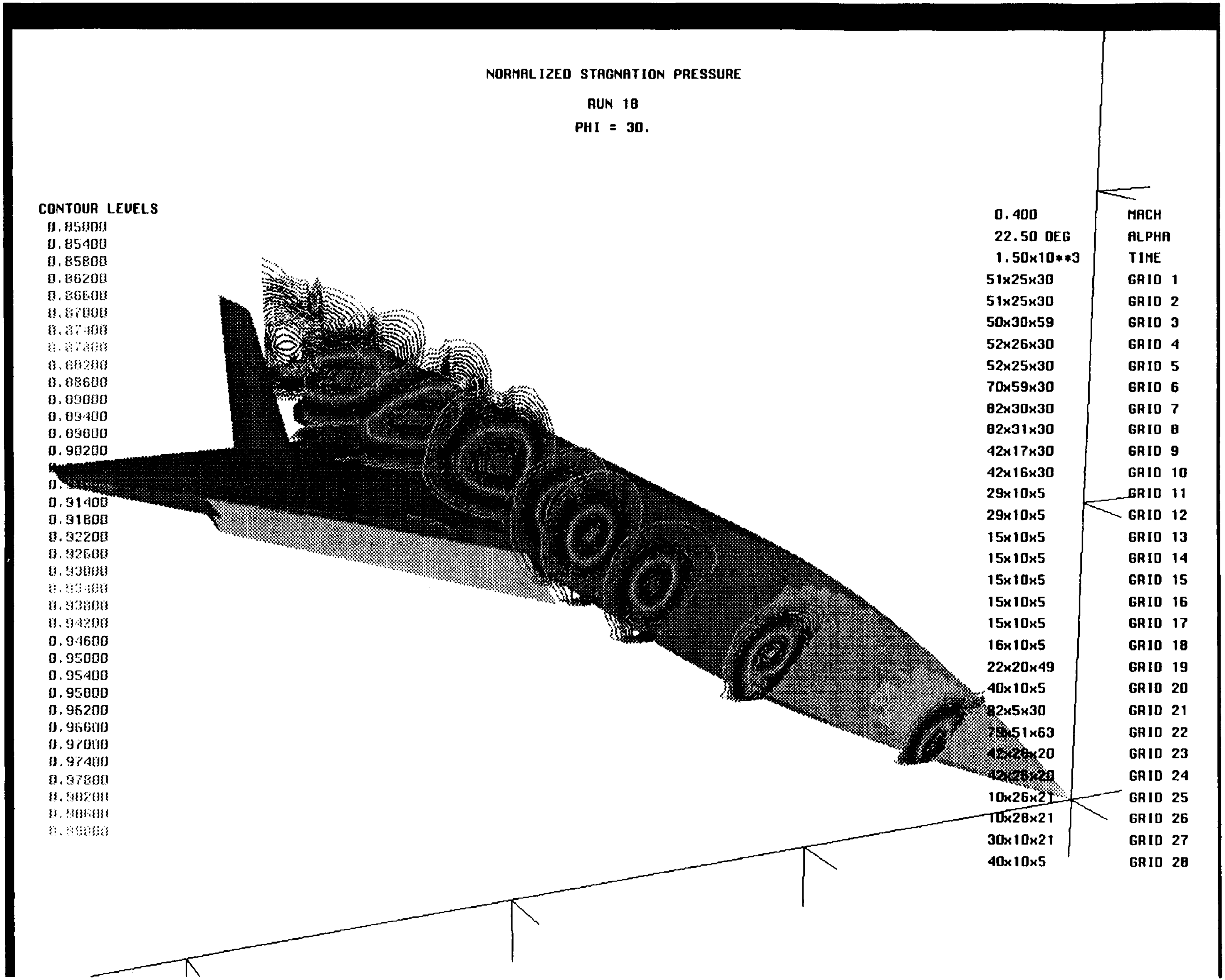

Figure 26. Stagnation Pressure Contours, phi=30 deg., alpha=22.5 deg.

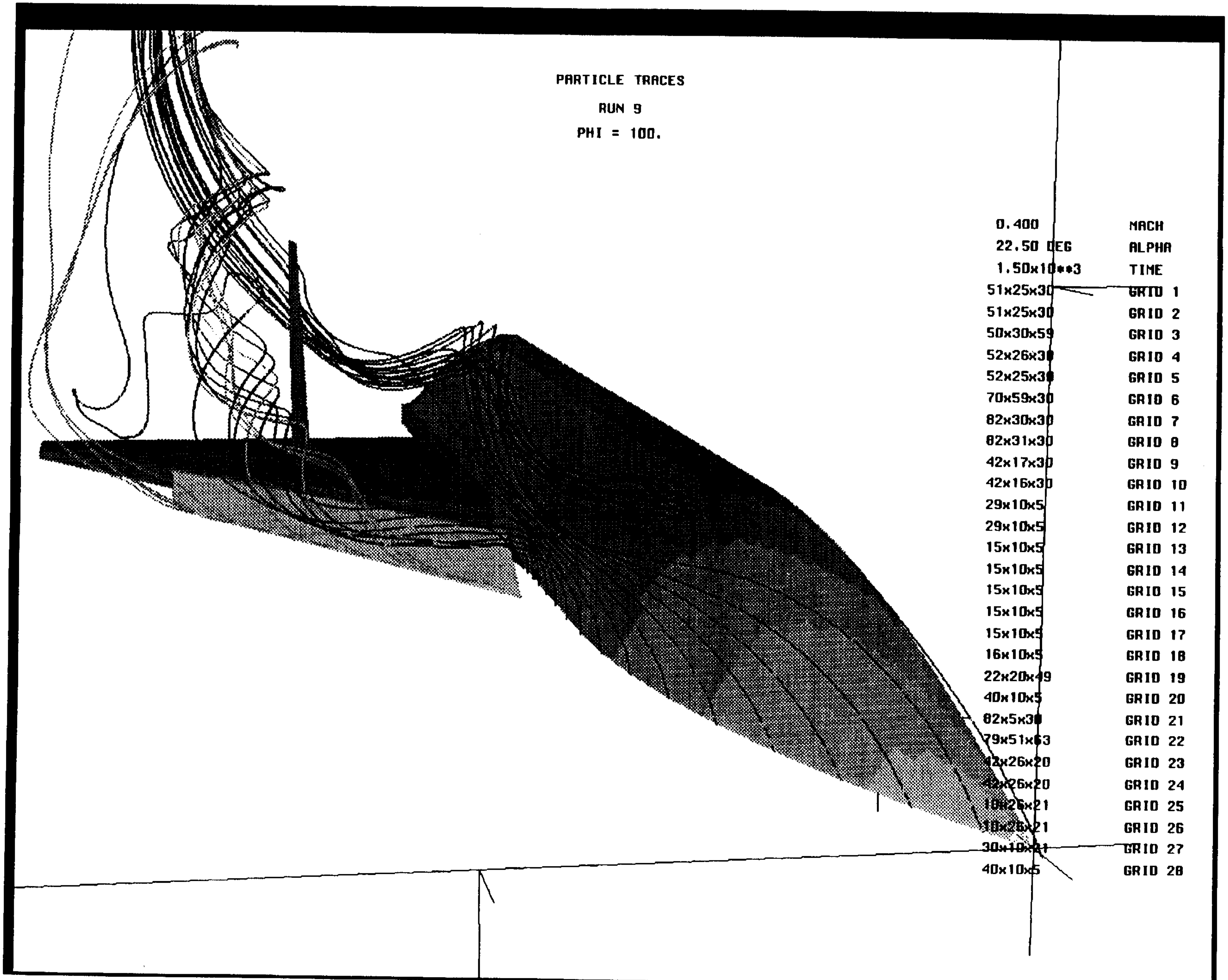

Figure 27. Particle Traces, phi=100 deg., alpha=22.5 deg.

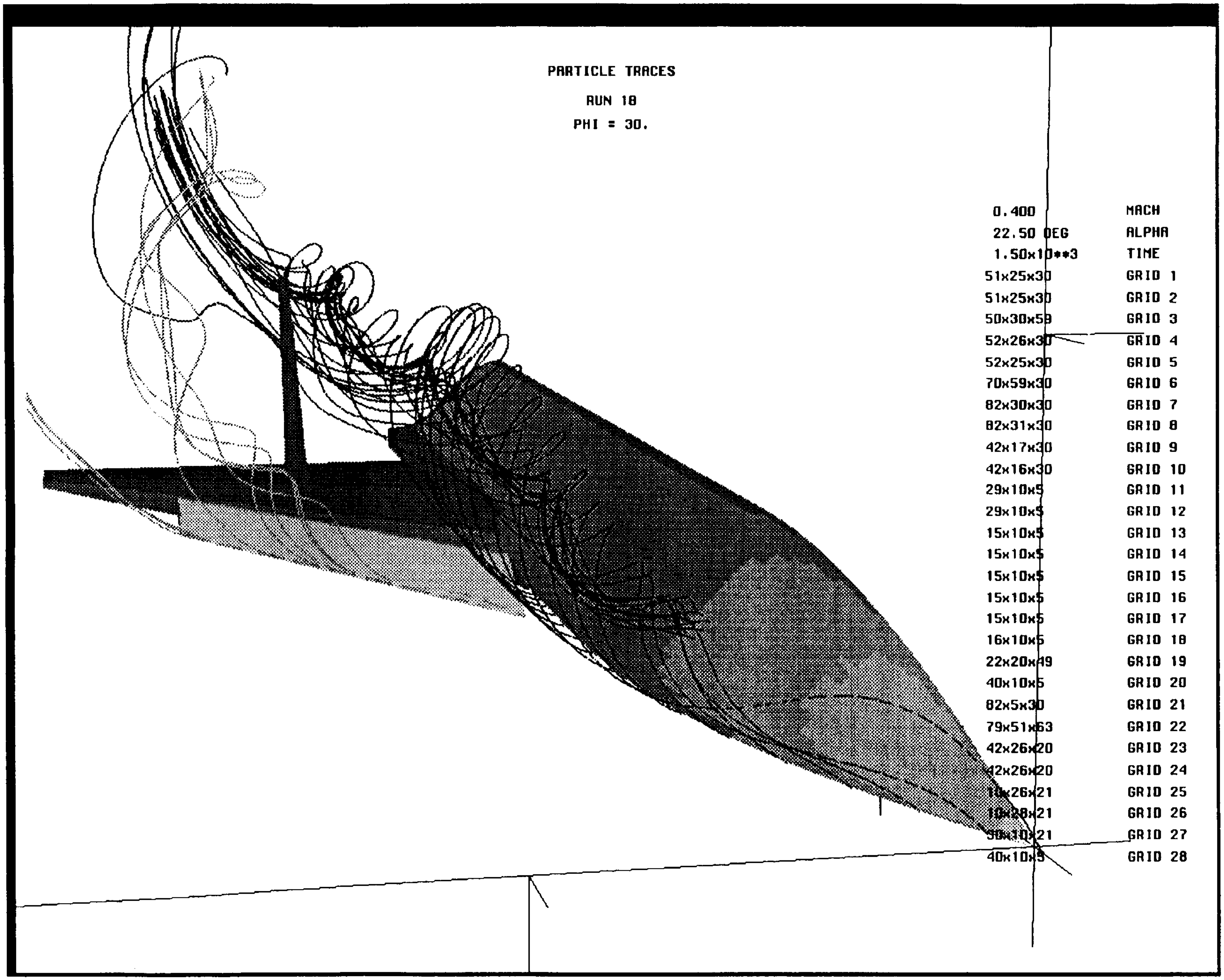

Figure 28. Particle Traces, phi=30 deg., alpha=22.5 deg.

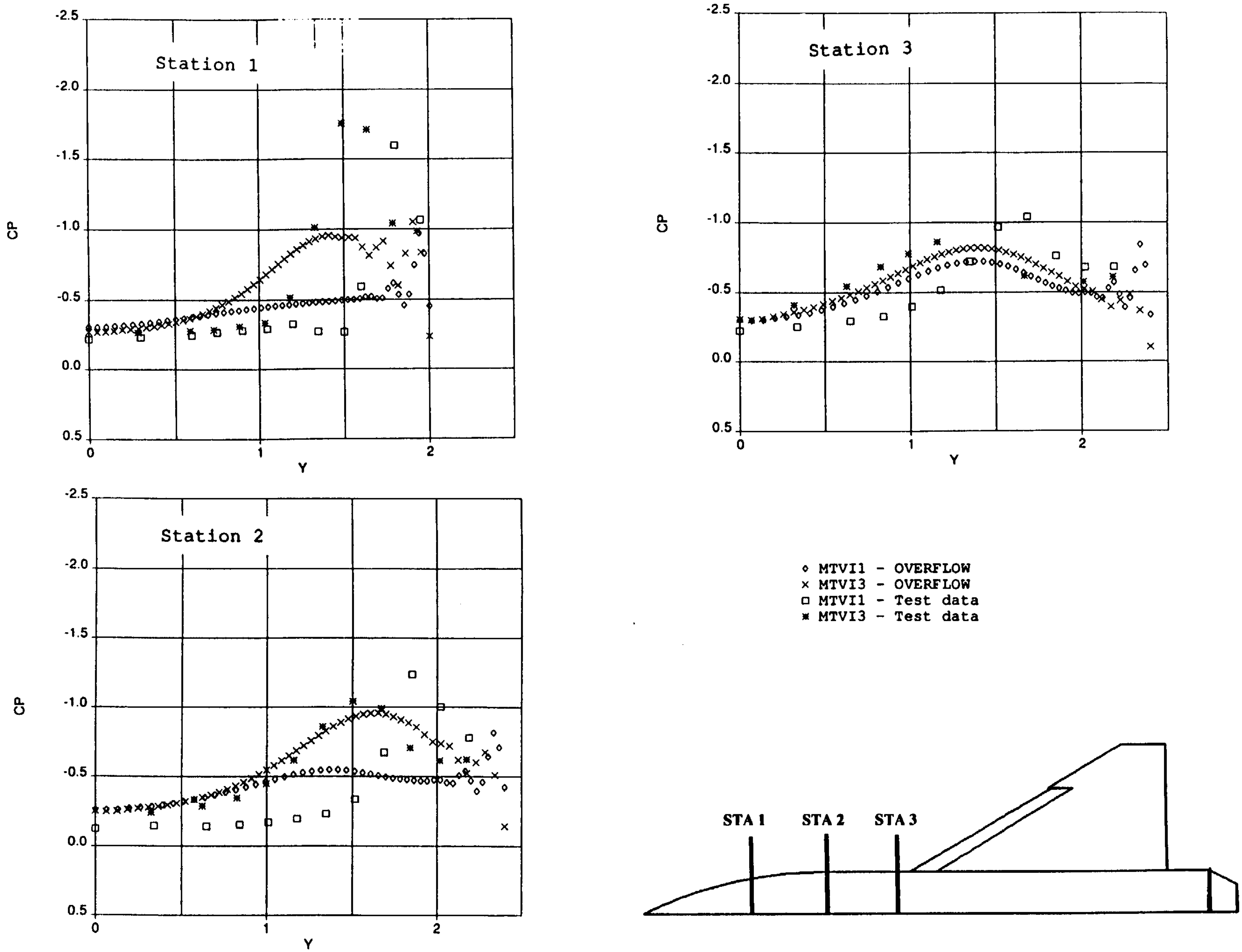

Figure 29. Upper Surface Forebody Pressure Coefficient, alpha=22.5 deg.

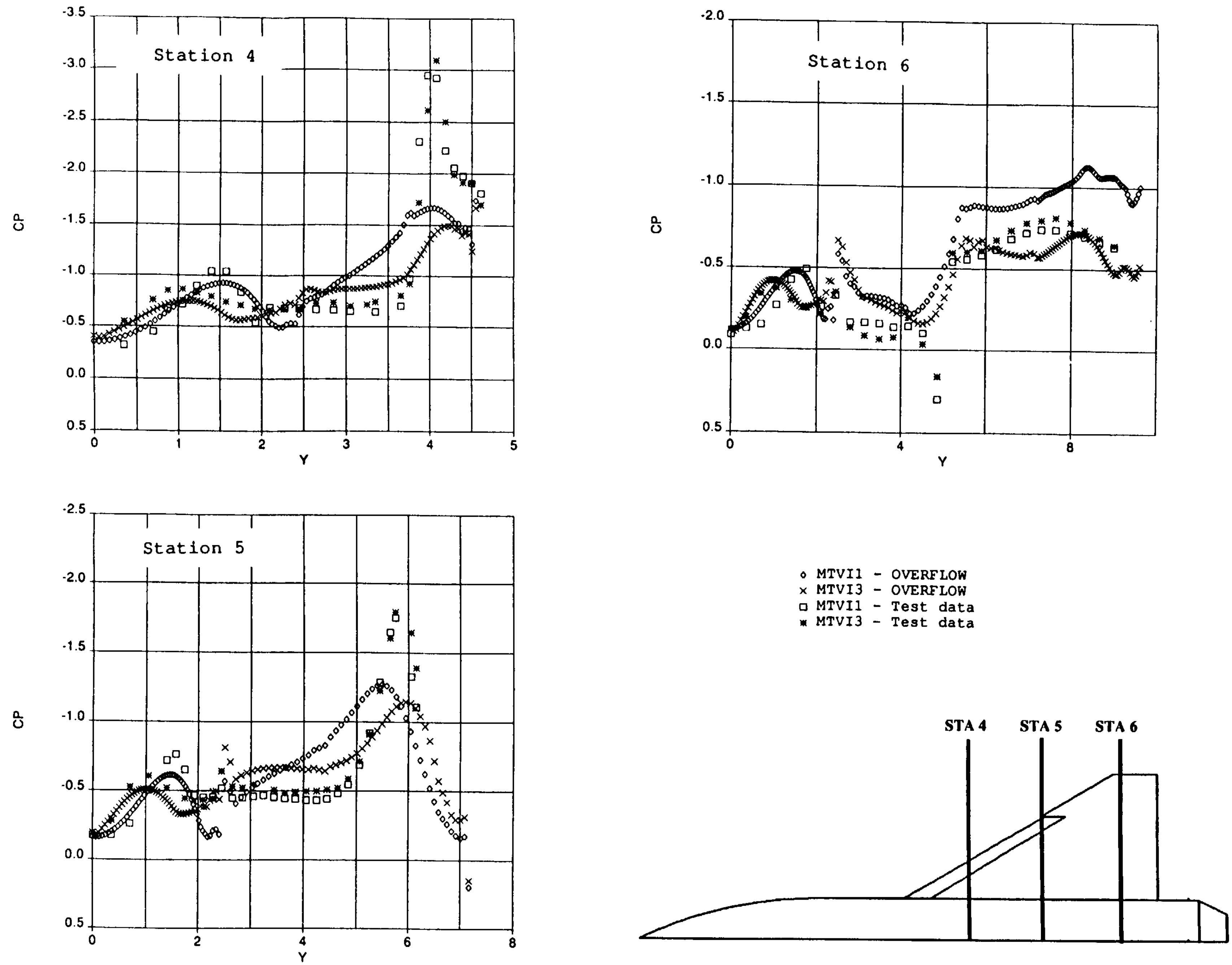

Figure 30. Upper Surface Wing Pressure Coefficient, alpha=22.5 deg.

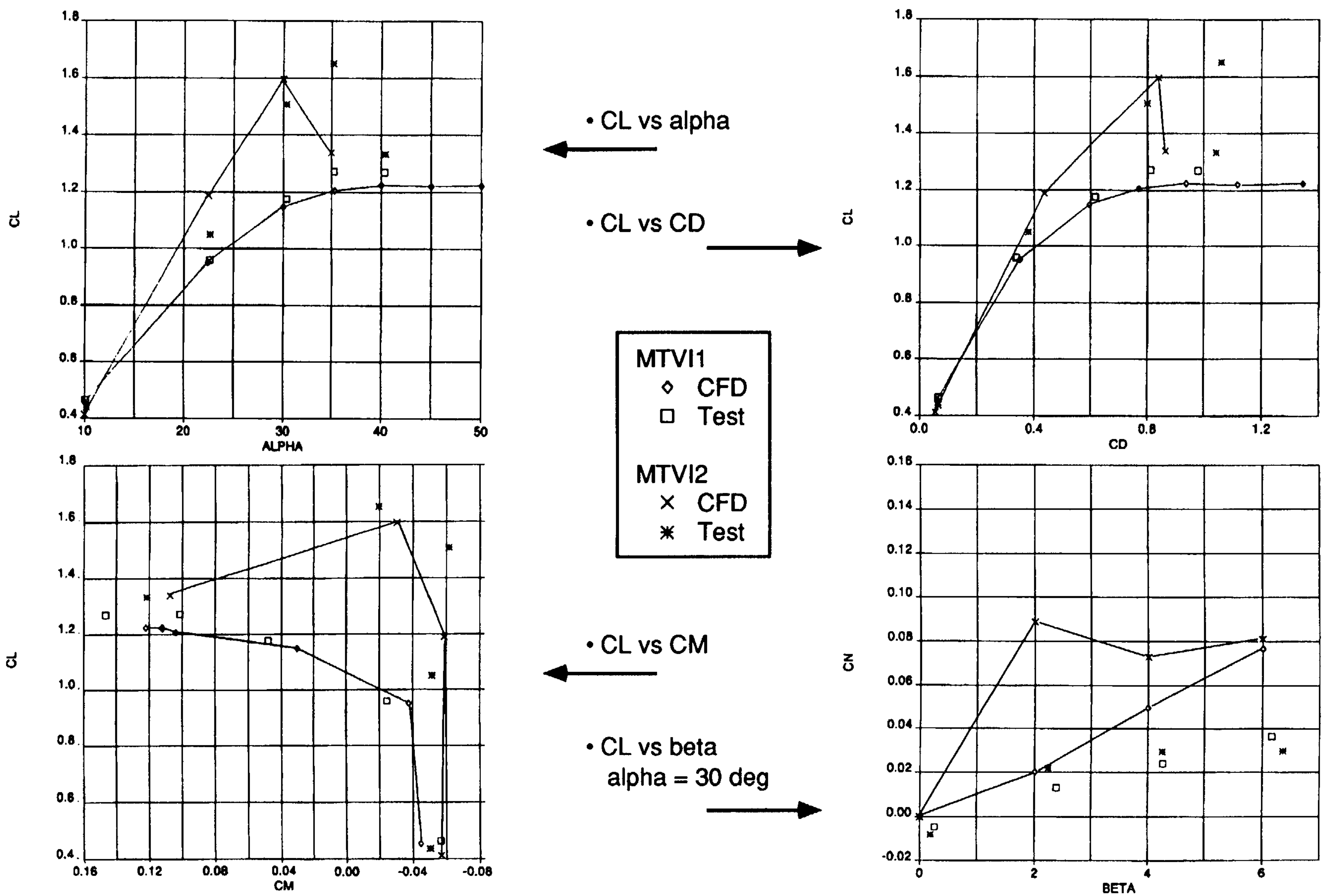

Figure 31. Effect of Vertical Tail Configuration and Sideslip Angle

spb-8-7-bh-C3a

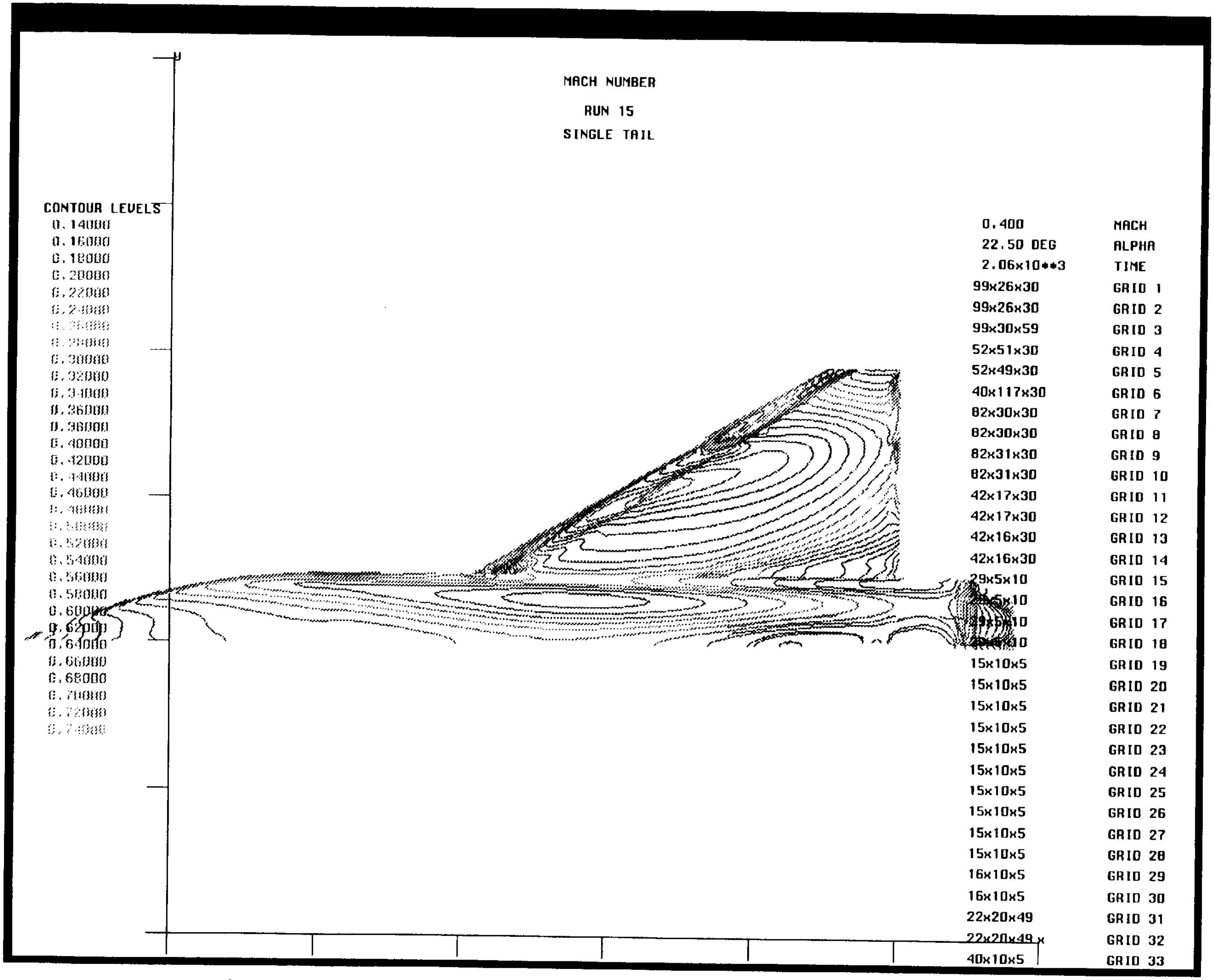

Figure 32. Upper Surface Mach Number Contours, MTVI2, alpha=22.5 deg.

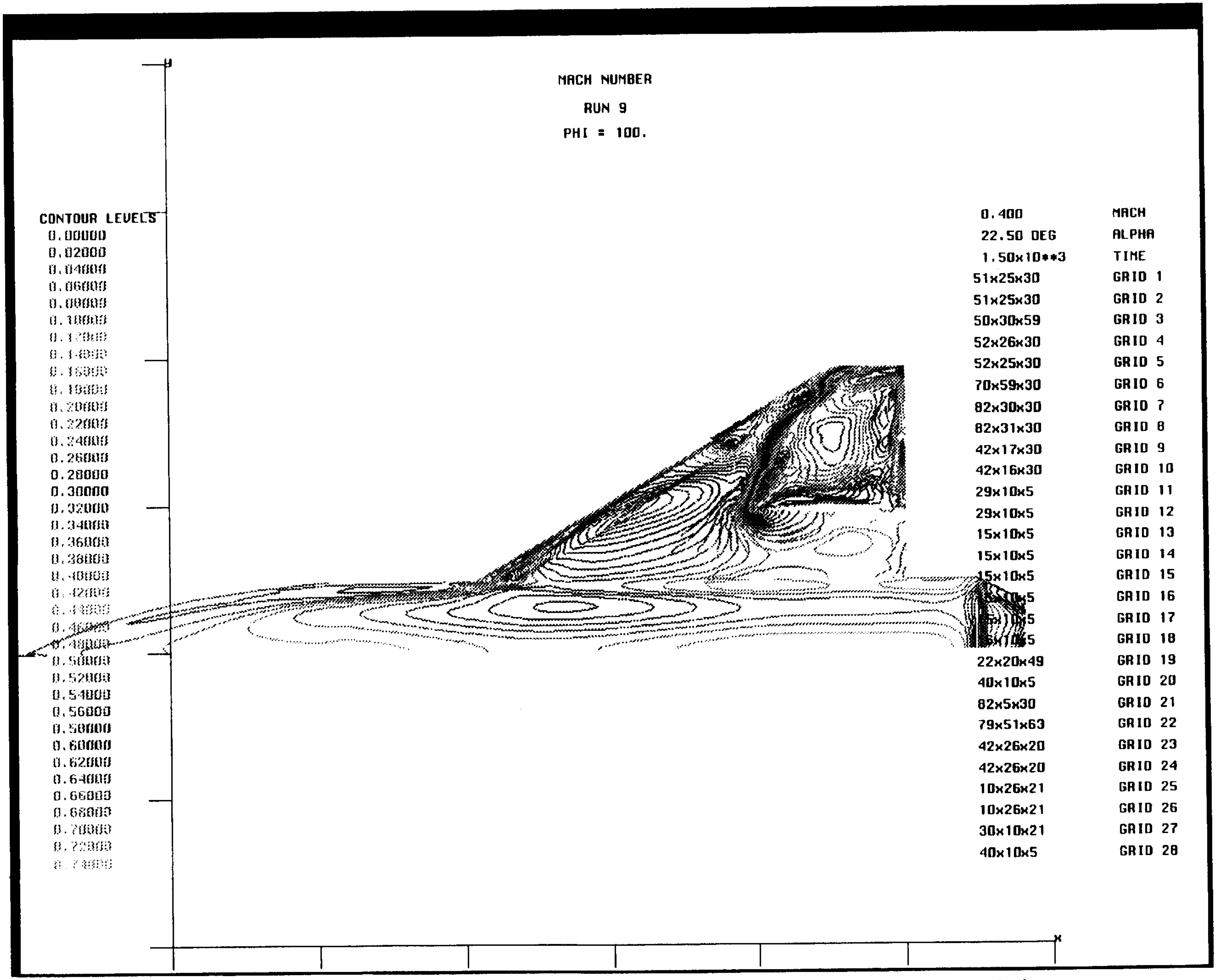

Figure 33. Upper Surface Mach Number Contours, MTVI1, alpha=22.5 deg.

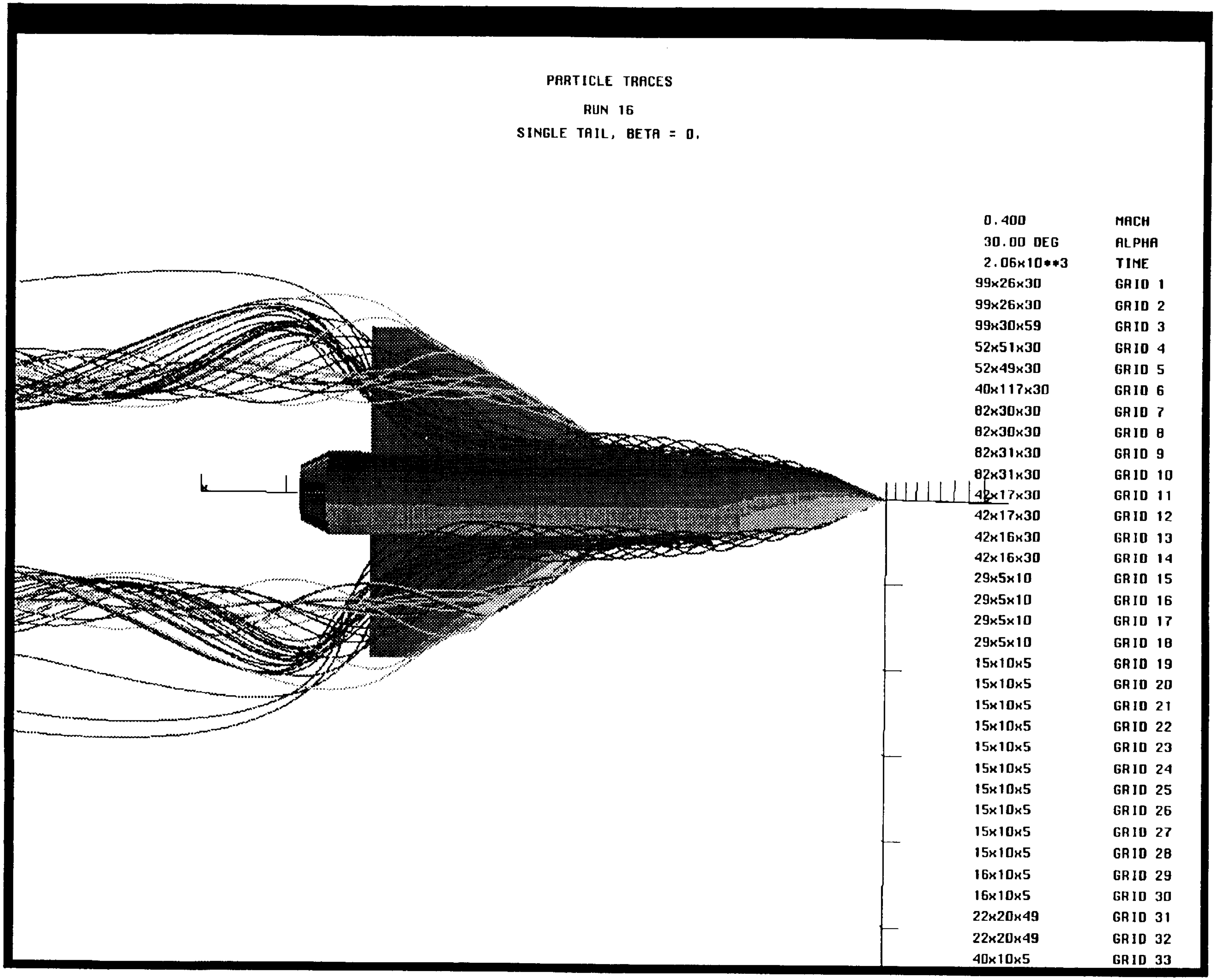

Figure 34. Particle Traces, MTVI2, alpha=30 deg.

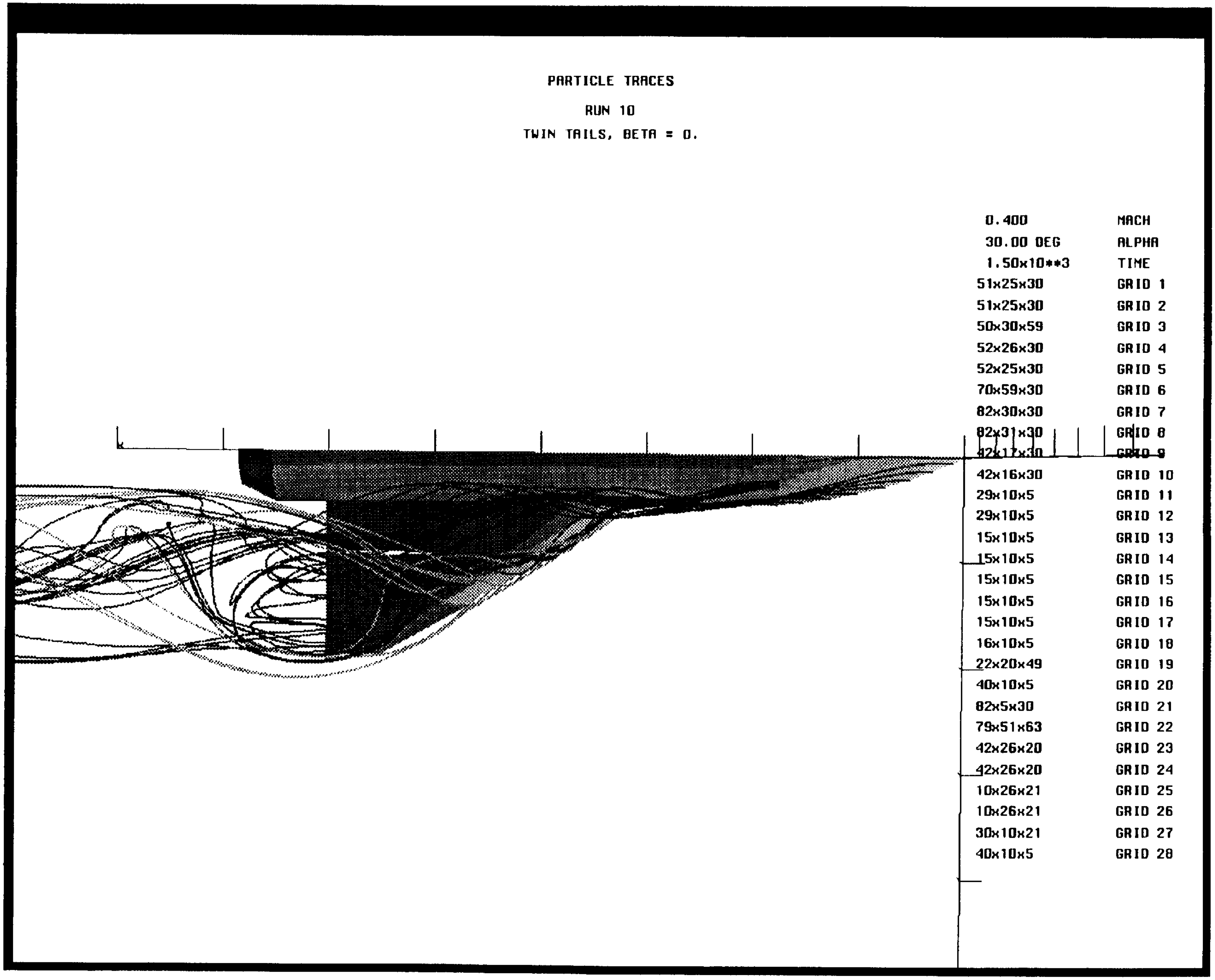

Figure 35. Particle Traces, MTVI1, alpha=30 deg.

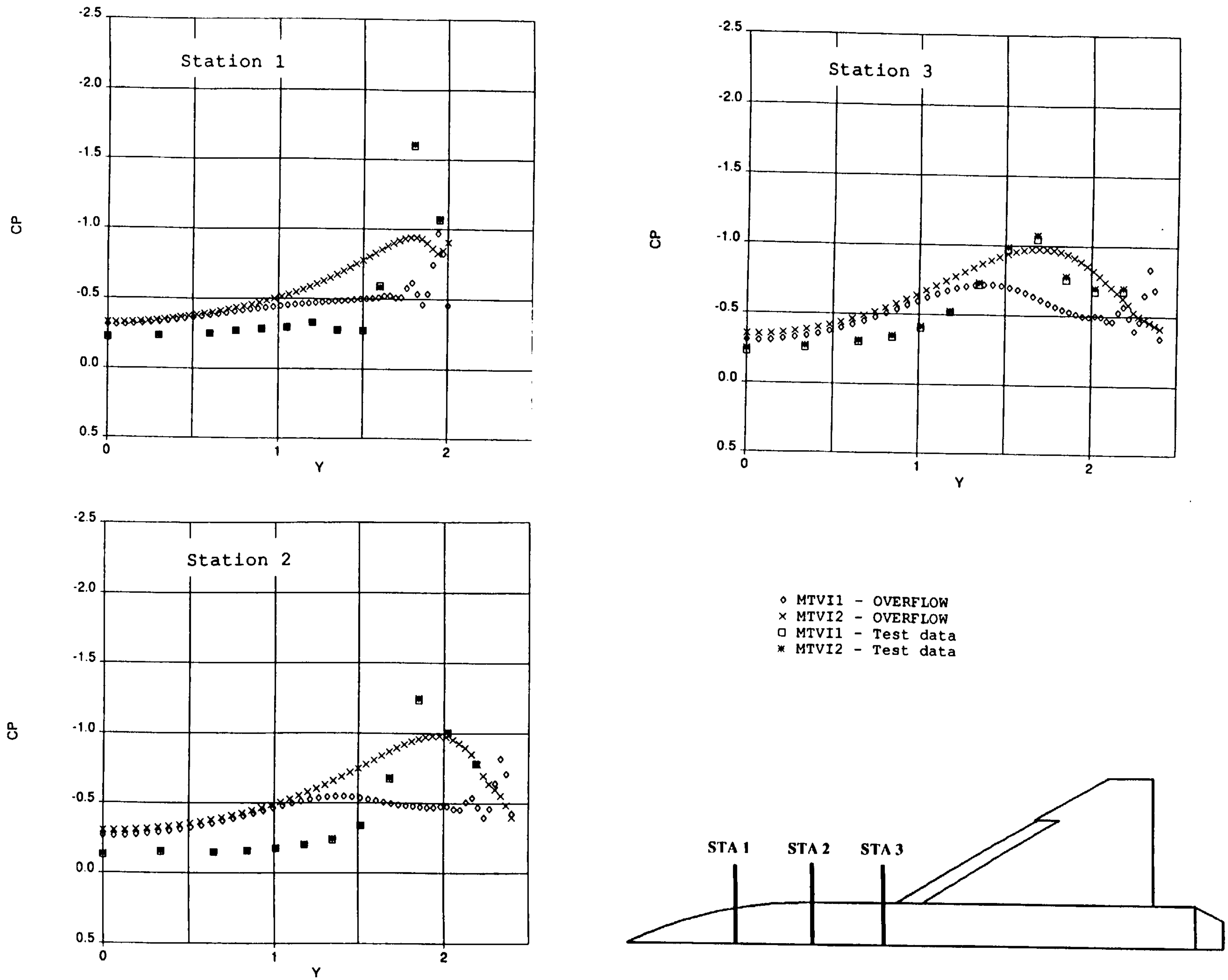

Figure 36. Upper Surface Forebody Pressure Coefficient, alpha=22.5 deg.

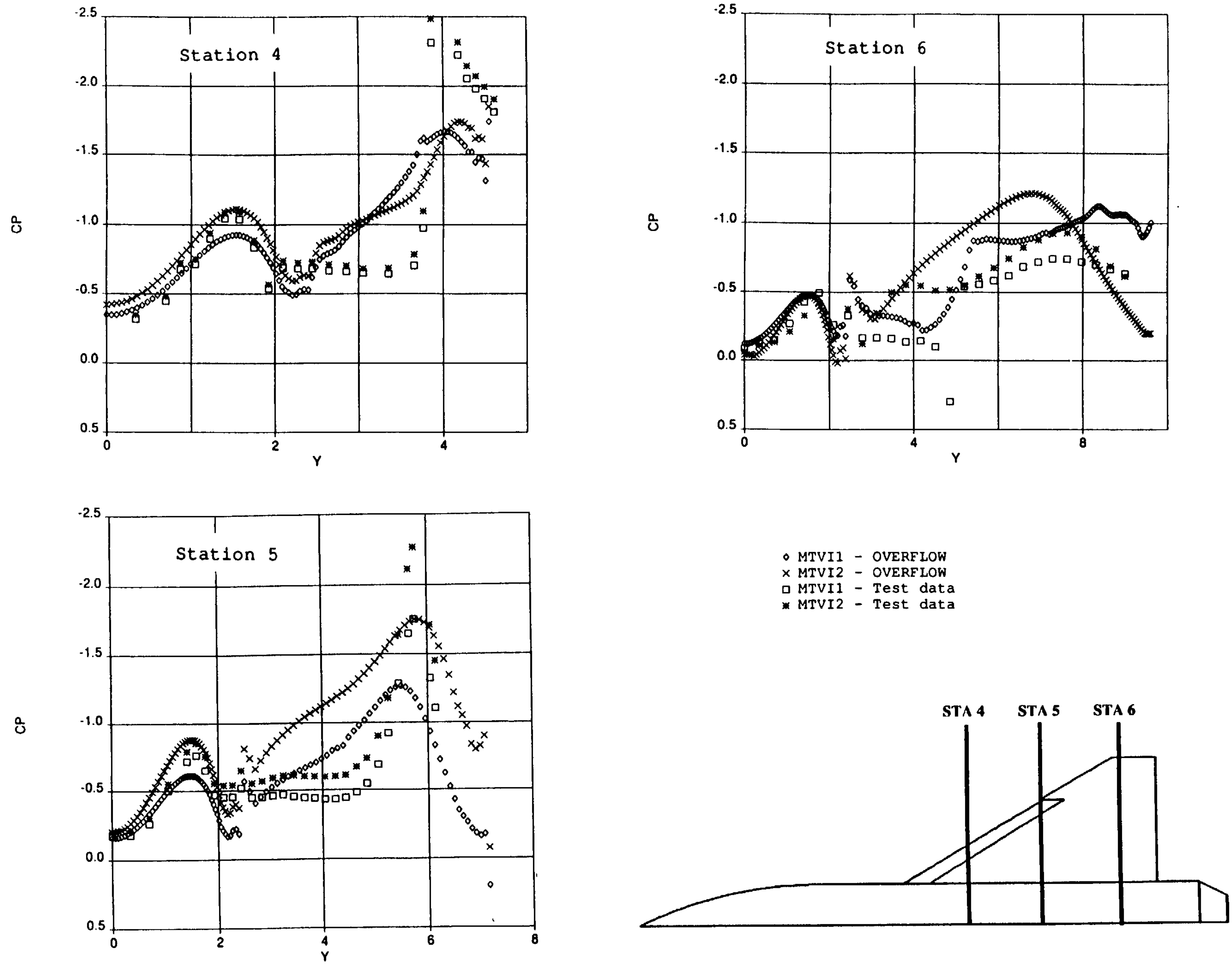

Figure 37. Upper Surface Wing Pressure Coefficient, alpha=22.5 deg.

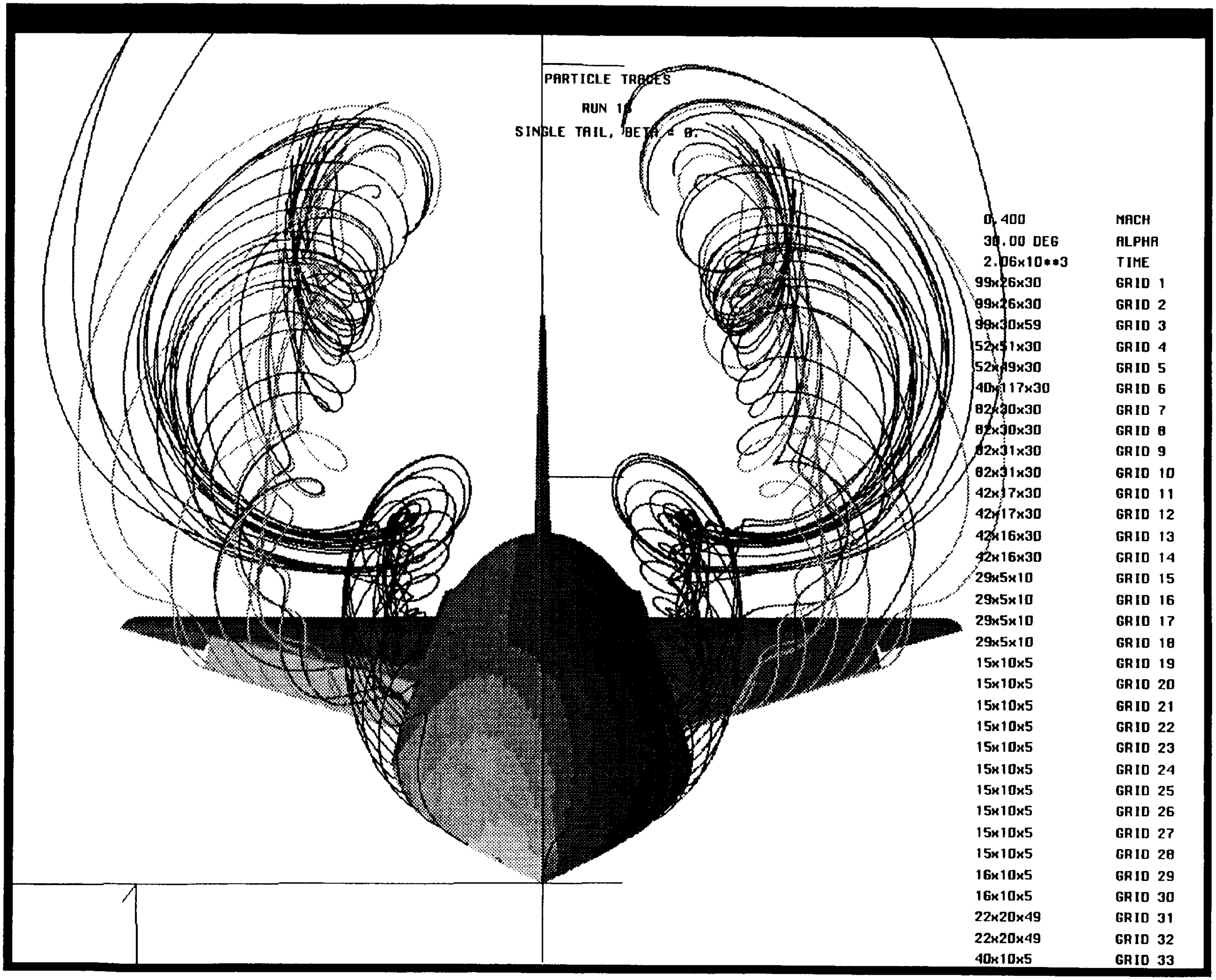

Figure 38. Particle Traces, MTVI1, alpha=30 deg., beta=0 deg.

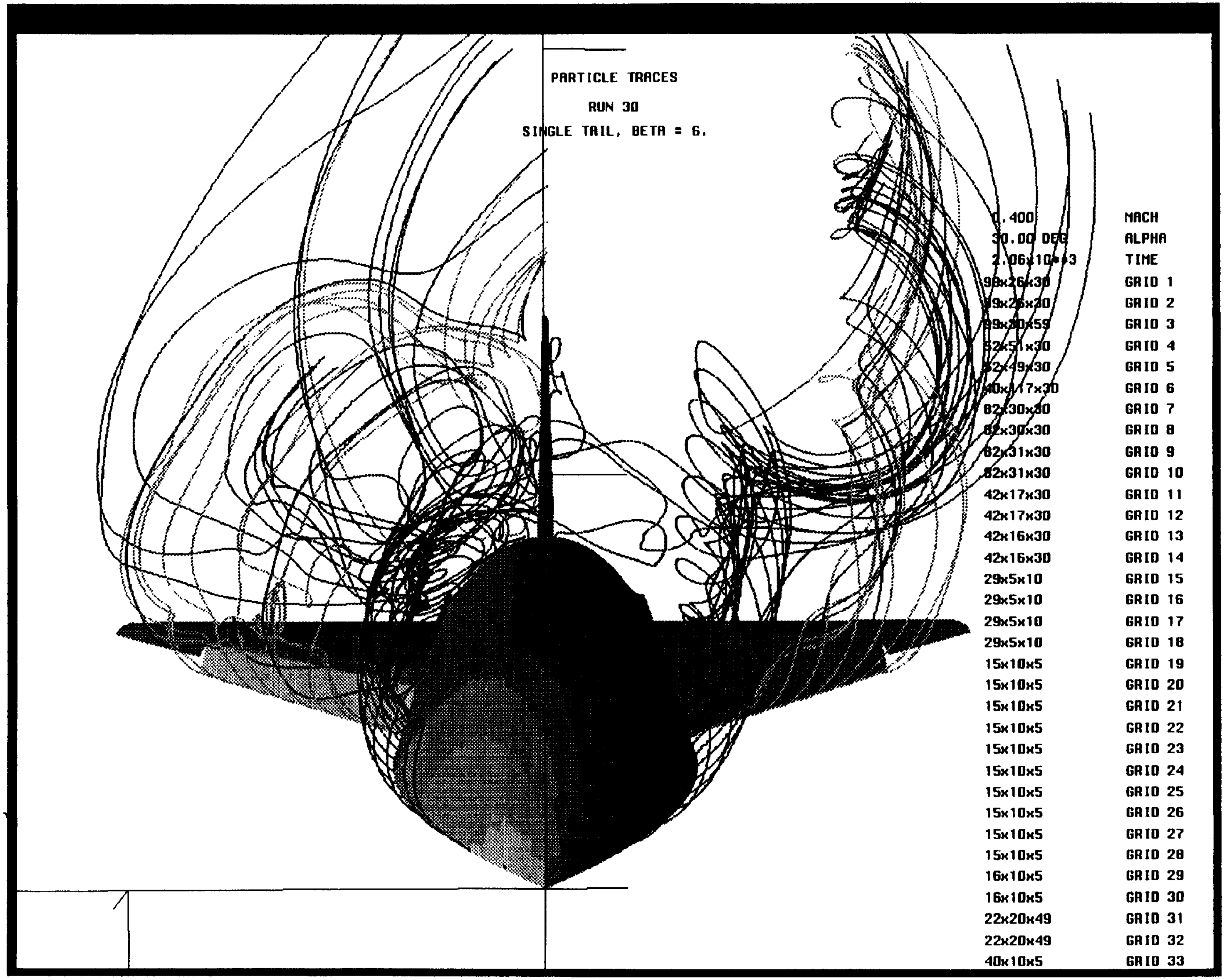

Figure 39. Particle Traces, MTVI1, alpha=30 deg., beta=6 deg.

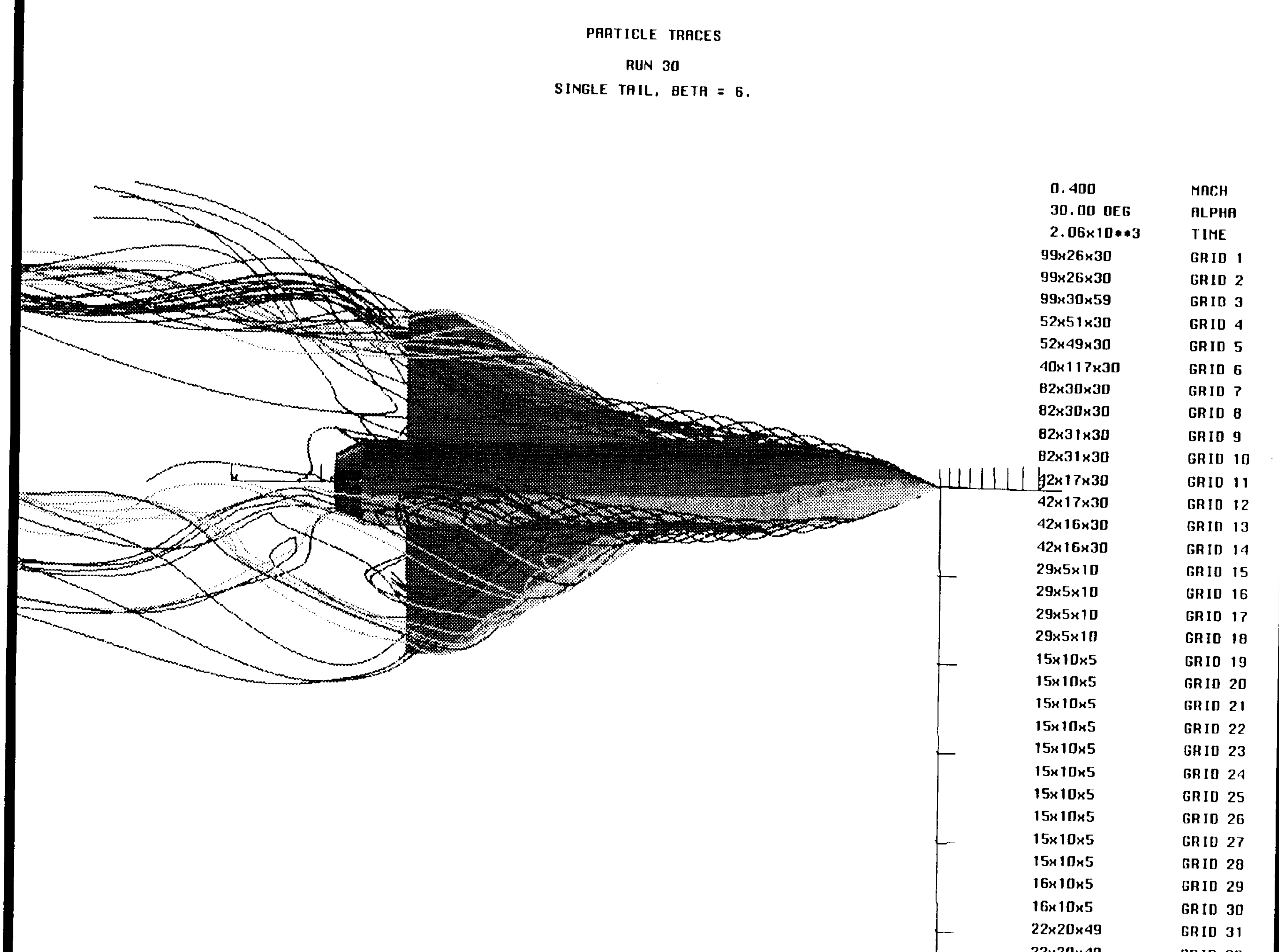

Figure 40. Particle Traces (planview), MTVI1, alpha=30 deg., beta=6 deg.

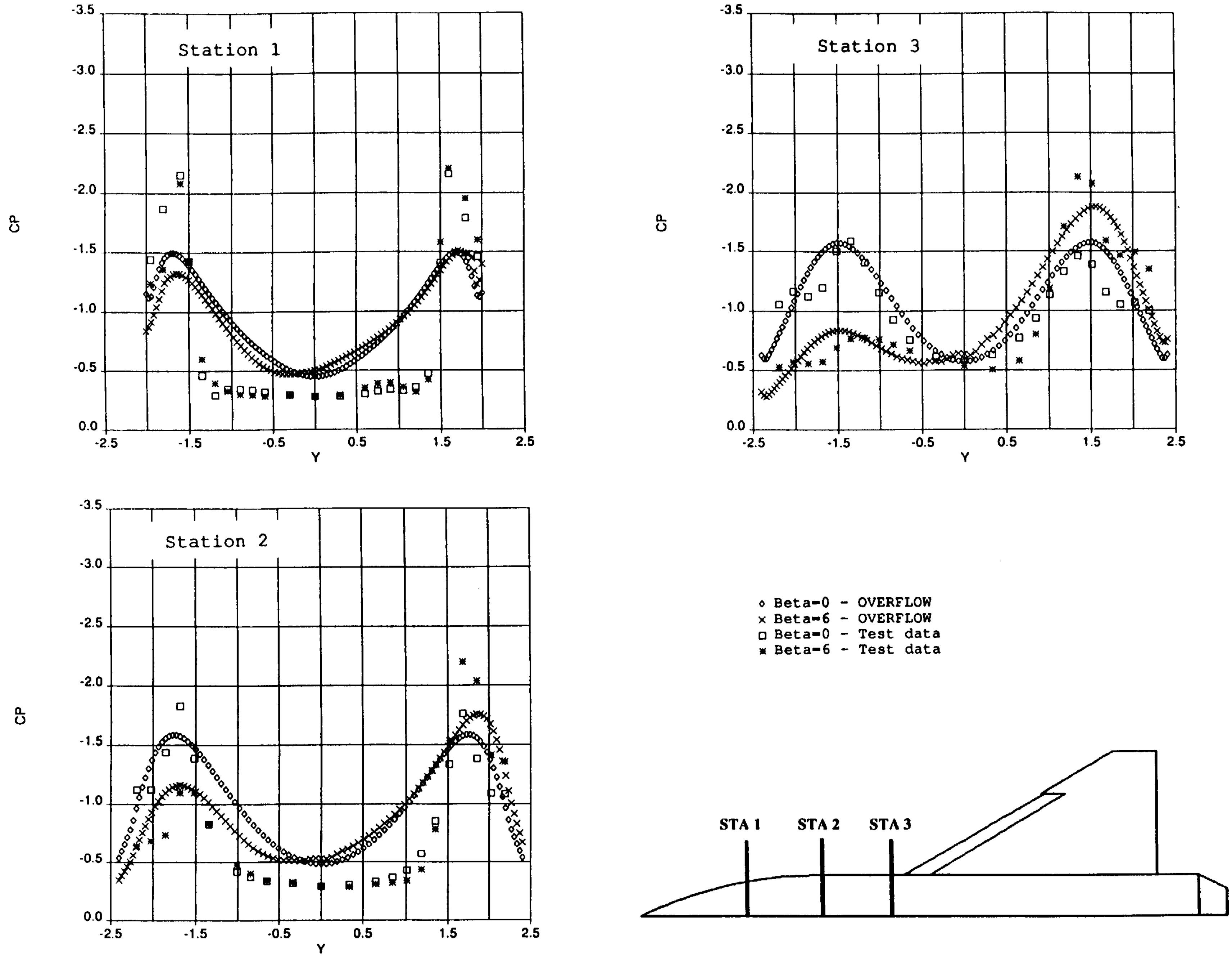

Figure 41. Upper Surface Forebody Pressure Coefficient, MTVI2, alpha=30. deg.

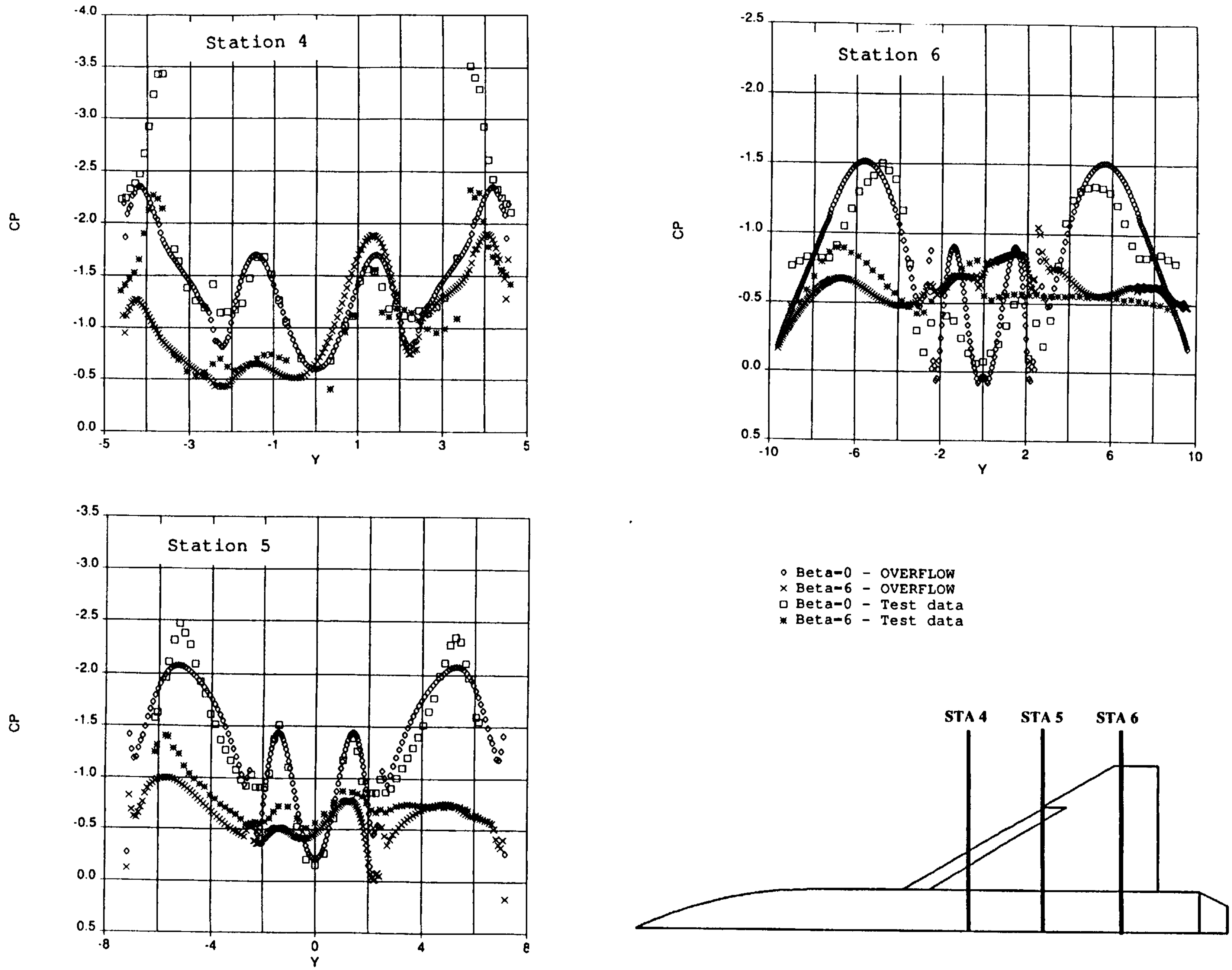

Figure 42. Upper Surface Wing Pressure Coefficient, MTVI2, alpha-30. deg.

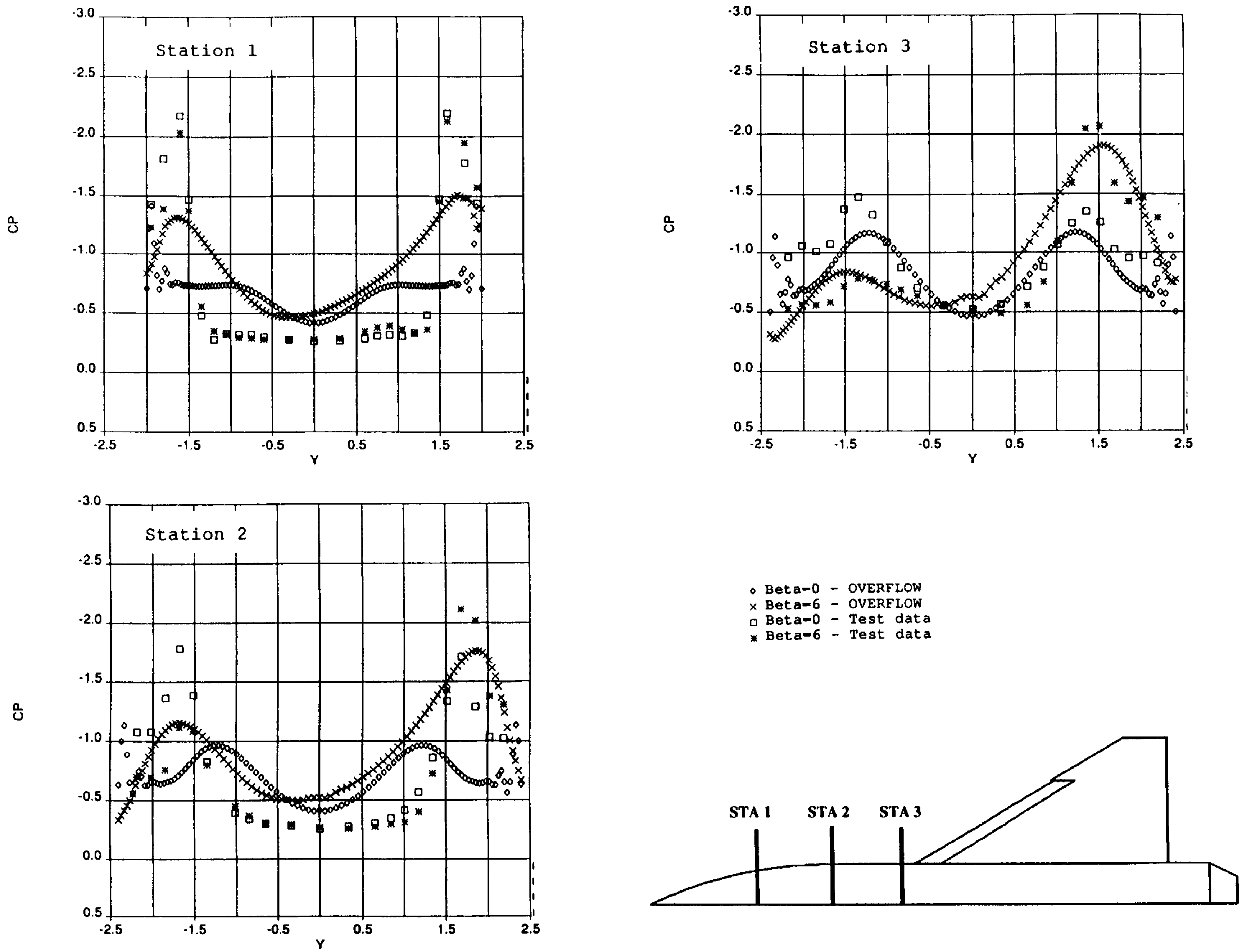

Figure 43. Upper Surface Forebody Pressure Coefficient, MTVI1, alpha=30. deg.

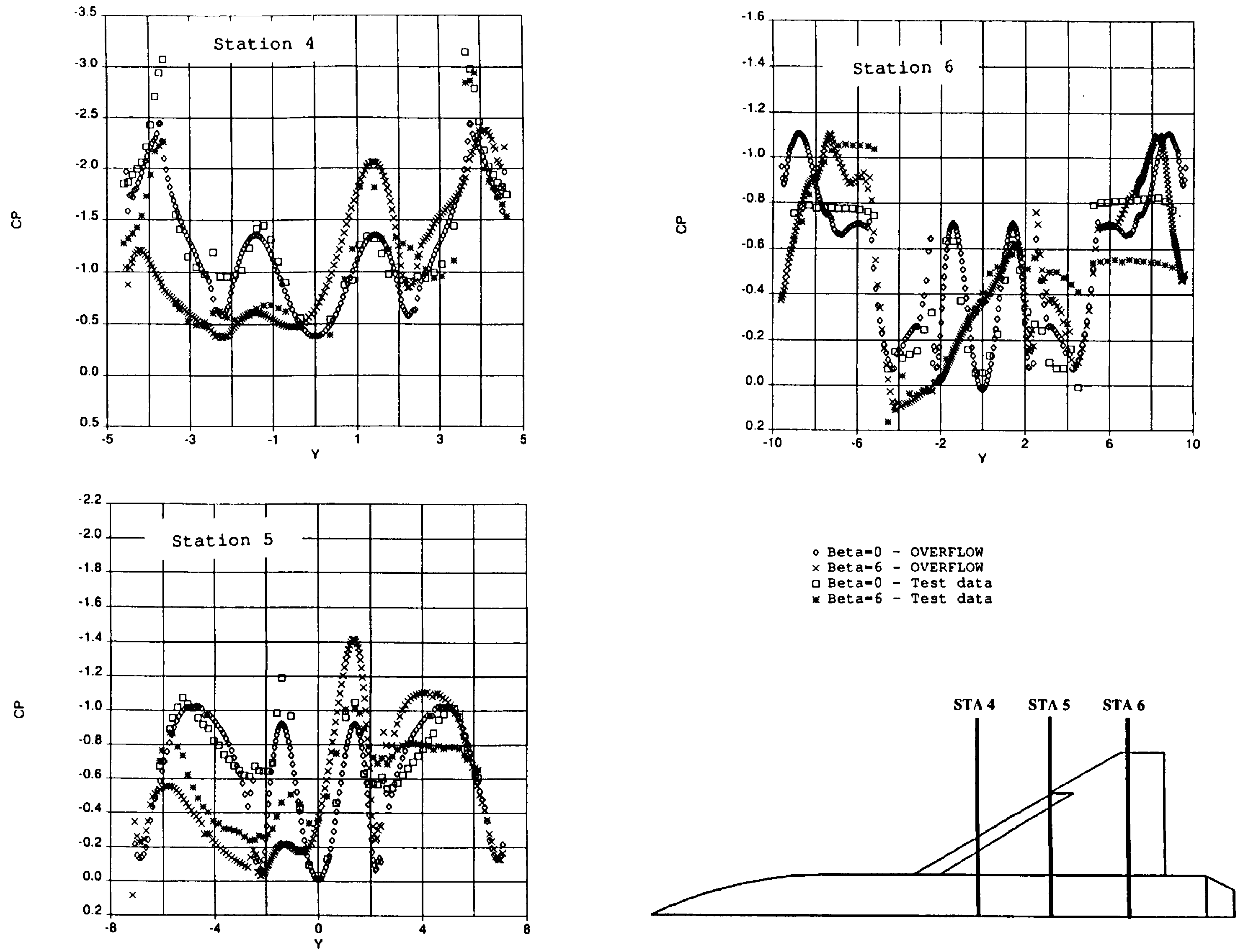

Figure 44. Upper Surface Wing Pressure Coefficient, MTVI1, alpha=30. deg.

REPORT DOCUMENTATION PAGE

Form Approved
OMB No. 0704-0188

1. AGENCY USE ONLY *(Leave blank)*

2. REPORT DATE
March 1995

3. REPORT TYPE AND DATES COVERED
Contractor Report (2/1/94 to 8/1/94)

4. TITLE AND SUBTITLE
Euler Technology Assessment for Preliminary Aircraft Design Employing OVERFLOW Code with Multiblock Structured-Grid Method

5. FUNDING NUMBERS
C NAS1-18762, Task 26
WU 505-68-30-03

6. AUTHOR(S)
David A. Treiber and Dennis A. Muilenburg

7. PERFORMING ORGANIZATION NAME(S) AND ADDRESS(ES)
Boeing Defense & Space Group
Seattle, WA 98124-2207

8. PERFORMING ORGANIZATION REPORT NUMBER

9. SPONSORING/MONITORING AGENCY NAME(S) AND ADDRESS(ES)
National Aeronautics and Space Administration
Langley Research Center
Hampton, VA 23681-0001

10. SPONSORING/MONITORING AGENCY REPORT NUMBER
NASA CR-4651

11. SUPPLEMENTARY NOTES
Technical Monitor: Mr. Farhad Ghaffari
NASA Langley Research Center
Hampton VA 23681-0001

12a. DISTRIBUTION/AVAILABILITY STATEMENT
Unclassified-Unlimited
Subject Category 02

12b. DISTRIBUTION CODE

13. ABSTRACT *(Maximum 200 words)*

The viability of applying a state-of-the-art Euler code to calculate the aerodynamic forces and moments through maximum lift coefficient for a generic sharp-edge configuration is assessed. The OVERFLOW code, a method employing overset (Chimera) grids, was used to conduct mesh refinement studies, a wind-tunnel wall sensitivity study, and a 22-run computational matrix of flow conditions, including sideslip runs and geometry variations. The subject configuration was a generic wing-body-tail geometry with chined forebody, swept wing leading-edge, and deflected part-span leading-edge flap. The analysis showed that the Euler method is adequate for capturing some of the non-linear aerodynamic effects resulting from leading-edge and forebody vortices produced at high angle-of-attack through C_{Lmax}. Computed forces and moments, as well as surface pressures, match well enough useful preliminary design information to be extracted. Vortex burst effects and vortex interactions with the configuration are also investigated.

14. SUBJECT TERMS
Computational Fluid Dynamics, Euler formulation, Preliminary aircraft design, Sharp-edge flow-separation, Vortex flow, Vortex burst, Vortex burst, OVERFLOW

15. NUMBER OF PAGES
66

16. PRICE CODE
A04

17. SECURITY CLASSIFICATION OF REPORT	18. SECURITY CLASSIFICATION OF THIS PAGE	19. SECURITY CLASSIFICATION OF ABSTRACT	20. LIMITATION OF ABSTRACT
Unclassified	Unclassified	Unclassified	